MOUNTAIN-PLAINS CONSORTIUM

MPC 15-292 | T. Sobieck, R. Atadero and H. Mahmoud

Predicting Fatigue Service Life Extension of RC Bridges with Externally Bonded CFRP Repairs

A University Transportation Center sponsored by the U.S. Department of Transportation serving the Mountain-Plains Region. Consortium members:

Colorado State University
North Dakota State University
South Dakota State University
University of Colorado Denver
University of Denver
University of Utah
Utah State University
University of Wyoming

Predicting Fatigue Service Life Extension of RC Bridges with Externally Bonded CFRP Repairs

Tyler Sobieck
Dr. Rebecca Atadero, PI
Dr. Hussam Mahmoud

Department of Civil and Environmental Engineering
Colorado State University

December 2015

Acknowledgements

The authors would like to thank Fyfe Co. for their generous donation of all composite materials, and the staff at the Colorado State University Engineering Research Center for assistance in performing the experimental testing.

Disclaimer

The contents of this report reflect the views of the authors, who are responsible for the facts and the accuracy of the information presented. This document is disseminated under the sponsorship of the Department of Transportation and the University Transportation Centers Program in the interest of information exchange. The U.S. Government assumes no liability for the contents or use thereof.

ABSTRACT

This paper presents the results of an experimental study on the fatigue performance of RC beams strengthened with different externally bonded CFRP systems. Seven specimens were fabricated; three had no CFRP; the remaining four had one of two CFRP systems. The objective of this study was to determine the effect the CFRP repair had on the growth rate of a fatigue crack initiating from a notch in the tensile rebars. The results of the experimental study showed an extended fatigue life and a slowed crack growth rate in specimens repaired with both CFRP systems. The crack growth rates were used to determine material constants for the Paris Law, which describes growth of a stable fatigue crack. These results were then used to propose recommendations for design of FRP repair systems for a specific fatigue life.

TABLE OF CONTENTS

LIST OF TABLES

LIST OF FIGURES

EXECUTIVE SUMMARY

A majority of the United States' transportation infrastructure is over 50 years old with one in nine bridges being considered structurally deficient. Fatigue damage accumulation in bridge structures, generated by cyclic loading of passing traffic, has led to shorter service lives. Over the past few decades, studies have shown carbon fiber reinforced polymer (CFRP) repairs to be an effective means of reducing fatigue damage accumulation in reinforced concrete (RC) girders. Despite the abundant research, the results, specifically the increase in fatigue life, vary widely making it difficult to apply them directly to repair designs. Therefore, design codes and guidelines presently in use are insufficient in providing engineers with the proper information to determine the extended fatigue life of the RC bridges repaired with CFRP.

Current design codes state FRP repairs should limit the stress range in the reinforcing bars below the threshold where fatigue cracks can propagate. The problem with this philosophy is it essentially designs an overly conservative system with an infinite fatigue life. The proposed approach follows a performance based-design philosophy for which the engineer designs for a specified extension in service life by limiting the crack growth rate in the reinforcement so the critical crack length, for which fracture in the reinforcement would occur, is never reached in the extended life.

In this report, the results of experimental fatigue testing of full scale control and CFRP repaired RC beams are highlighted and the fatigue crack propagation rate in the steel reinforcement is assessed for different repair schemes. The focus on steel reinforcement crack propagation rates was made because similar studies have found the reinforcement to be the limiting fatigue component in RC bridge girders. Two different CFRP systems were used for repair, two beams with each kind. The beams were repaired so both systems had the same flexural capacity in order to determine if, despite the same strength, the fatigue lives differed. Measurement of the fatigue crack growth rate in the tensile reinforcement was performed using a visual method, which required the removal of a small portion of the concrete cover at mid-span of the beam. To ensure fatigue crack propagation at the location where the crack could be visually monitored, a notch was cut into the tensile reinforcement, which represented a corrosion pit forming over a decade.

The results of the experimental study showed an extended fatigue life and a slowed crack growth rate in specimens repaired with both CFRP systems. The results were inconclusive in indicating which CFRP system improved the fatigue performance the most. The measured crack growth rates were used to determine the material constants for the Paris Law, which describes growth of a stable fatigue crack. These determined values were reasonably close to well established values for this type of steel. The tensile reinforcement stress range, Paris Law material constants, and crack growth rate data were then used to propose recommendations for design of FRP repair systems for RC flexural members for a specific fatigue life using the combination of fracture mechanics and provisions from ACI 440.2 *Guide for the Design and Construction of Externally Bonded FRP Systems for Strengthening Concrete Structures*. The proposed design is presented in the form of a flow chart. Evaluation of the proposed design process was then performed using the experimental fatigue data, and a reasonable estimation of the extended fatigue life was determined.

1. INTRODUCTION

1.1 Background

Since 1998, the American Society of Civil Engineers has conducted an annual study providing information on the condition and performance of the United States infrastructure to the public in the form of report cards (ASCE 2013). These report cards, and recent structural failures, have shown the poor condition of our transportation infrastructure. One in nine of the nation's bridges are considered structurally deficient due to lack of funding for maintenance and repair, environmental degradation of structural components, and/or increased vehicular weight (ASCE 2013). In bridges, a large amount of the degradation is due to the hundreds of cyclic loading events that are experienced each day due to passing traffic. These cyclic loads lead to fatigue of the components in the structure. Fatigue is defined as cyclic loading producing stress ranges in a component well below its ultimate strength, resulting in microscopic damage accumulation until a crack develops, whose growth can lead to failure of the component (Dowling 1999). While fatigue is usually considered a more prominent problem in steel structures, the same concern is present in the steel reinforcing bars (rebar) in reinforced concrete (RC) beams.

While no structural failures have been reported as a result of fatigue in RC bridges, with the average age of the over 600,000 bridges in the U.S. being 42 years, replacement of many RC bridges with service lives of 50 years may soon need to occur. However, this option isn't always feasible with federal, state, and local departments of transportation (DOTs) struggling to procure the funding that is needed to address the deficient bridges, which the Federal Highway Administration estimates to be $20.5 billion annually to eliminate the backlog by 2028 (ASCE 2013). Therefore, a more economical, readily applicable, and durable repair method was needed.

Over the past couple decades, several systems have been developed and implemented in the field for repair of RC structures. Examples include enlarging the cross-sectional area of members, externally attaching steel plates to the tension soffit of the member, and most recently employing the use of fiber reinforced polymers (FRP). More focus has been shifted to the use of FRP systems due to the impracticality of increasing the member's cross-sectional area due to limited clearance and increased dead load, and the need of formwork for an extended amount of time when attaching steel plates (Jumaat et al. 2007).

FRP repair systems, which were originally developed in U.S., Canada, Switzerland, and Japan, excelled over other methods due to their lightweight, high strength, noncorrosive material and mechanical properties (Bank 2006). In addition FRPs have extremely high resistance to fatigue degradation. FRP sheet systems have the additional advantage of being able to take the form of almost any surface. For these reasons research looking at the fatigue performance of RC beams strengthened with FRP systems has increased in the past decade.

Studies researching this topic have led to design guidelines and state-of-the-art reports from the American Concrete Institute (ACI), the American Association of State Highway and Transportation Officials (AASHTO), and the National Cooperative Highway Research Program (NCHRP). These guidelines and the rapid expansion of FRP manufacturers have led many DOTs to look at the use of FRP systems for strengthening of RC bridges. However, the problem is that design guidelines currently available to engineers focus on providing increased strength with little guidance in addressing the critical fatigue component in RC bridges: the tensile reinforcement. Even when the codes do address fatigue of the steel reinforcement, the recommendations are overly conservative; additionally, the effects of pre-damage to the steel reinforcement aren't accounted for. Therefore, recommendations need to be developed that can

help engineersesigning FRP repairs of RC structures experiencing fatigue of the reinforcing steel with some degree of pre-damage from exposure to environmental attacks from in-service use.

1.2 Objectives

The significance of the current study is to experimentally determine the effect externally bonded CFRP repairs of RC girders have on the fatigue crack growth rate. The experimental program was designed to achieve the following objectives:

- Determine if addition of a CFRP repair can slow the fatigue crack growth rate and extend the fatigue life of a pre-damaged beam
- Determine the Paris Law material constants for steel reinforcing bars in RC beams repaired with CFRP
- Determine the validity of using Linear Elastic Fracture Mechanics (LEFM) and the Paris Law to predict the extended fatigue life a CFRP repair provides
- Develop fatigue limit state design recommendations for FRP repaired RC girders based on crack growth rate findings from the current study

1.3 Methods

In order to meet the objectives listed above, an experimental fatigue test program was designed and performed. Seven RC beams were designed, fabricated, and fatigue tested. Three beams had no external CFRP repair, two beams were repaired with a typical modulus CFRP sheet, and two were repaired with a high modulus CFRP strip. Additionally, one of the unrepaired beams was fabricated with no void in the concrete exposing the tensile rebars, while the rest of the beams did have a void. This void allowed for continuous monitoring of the fatigue crack growth throughout the test, as well as the effect this void had on the fatigue performance of the beam. Continuous monitoring of the fatigue crack growth would provide answers as to whether addition of FRP alters the crack growth rate. Additionally, strain gages, linear potentiometers, and an actuator mounted load cell provided the structural response of the test beams so determination of the fatigue parameters could be made. Fatigue life predictions using well-accepted and experimentally determined Paris Law constants would allow for justification of further use of these parameters and validation of the use of LEFM for predicting the fatigue life of RC member repaired with FRP. Once the use of these equations was confirmed, well-established equations for the strength design for FRP repairs of RC flexural members could be used, along with determined results to provide recommendations for FRP repairs of RC members based on a fatigue limit state.

1.4 Organization of Report

The presented report is broken into five sections. Section 1 provides an introduction on the study, giving a general overview of the problem to be addressed, background on the problem, and the significance of addressing this problem. It also lists the objectives of the study and the methods performed to address these objectives. Section 2 provides background information on FRPs, fatigue and fracture mechanics, existing studies focusing on the fatigue performance of FRP repaired RC beams, existing design guidelines, and methods for measuring fatigue crack growth. Section 3 details the experimental methods used to address gaps in the existing research, including small scale testing, full scale experimental test matrix, specimen design, specimen fabrication, material properties, test setup, and instrumentation. Section 4 provides the results of the experimental test and analysis of those results to validate the obtained values. Finally, Section 5 gives the proposed design recommendations based on the experimental results, conclusions of the study, and suggestions for future research.

2. LITERATURE REVIEW

2.1 Fiber Reinforced Polymers

Fiber reinforced polymers (FRPs) are composite materials, which means they are made from a combination of materials that have significantly different mechanical and/or chemical properties, that when combined, create a material with properties unique from the components that comprise it. As can be assumed from the name, FRPs are comprised of two materials: a polymer resin matrix and reinforcing fibers, as shown in Figure 2.1. The type of matrix and fiber, orientation of the fibers, as well as the ratio of matrix to fiber content will affect the properties of the FRP.

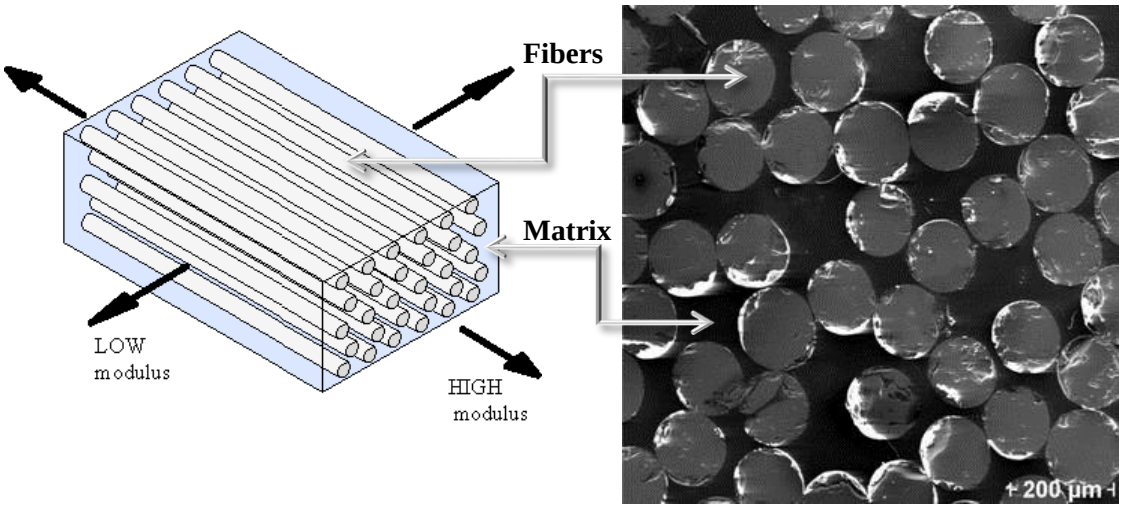

Figure 2.1 FRP composite material components (Gibson 1994)

2.1.1 Fibers

While many types of fibers exist, the most common types used in structural engineering applications are Aramid fibers (Kevlar) used in AFRP, carbon fibers used in making CFRP, and glass fibers used in making GFRP. Of the FRP fiber types, carbon has the greatest strength; typically 29,000-116,000 ksi, the highest modulus of elasticity, as well as the most resistance to fatigue failure in the fiber direction, with an endurance limit 60 – 70% of the initial static ultimate strength (ACI Committee 440.2R, 2008).

The single fiber filaments, once produced, can be post-processed into numerous different configurations as shown in Figure 2.2. For RC structure repairs the most common products are near surface mount rods, prepreg strips, and woven fabric sheets. The fibers in woven fabrics are typically orientated in a unidirectional (0^o) or bidirectional (0^o, 90^o or 45^o, -45^o) fashion. Unidirectional fabrics are primarily used in applications where tensile forces are only present in one direction, such as flexure of a beam.

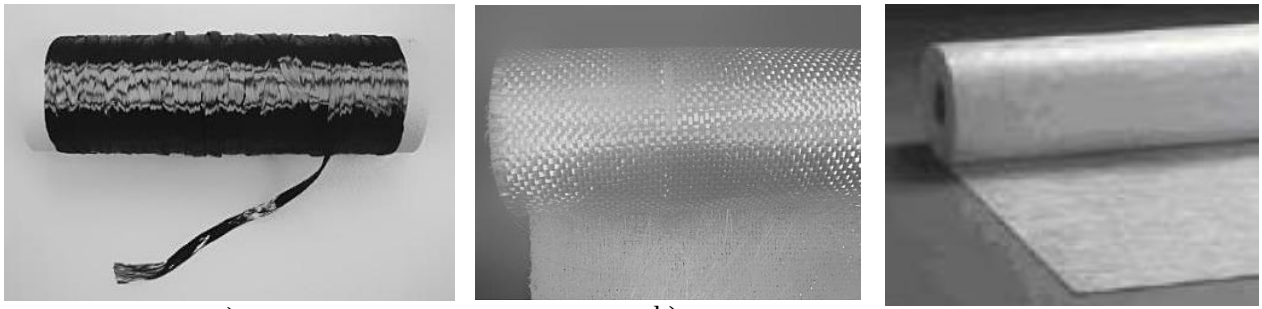

a) b) c)

Figure 2.2 Different types of FRP products: a) carbon fiber tow, b) glass fiber woven fabric, c) continuous glass filament mat (Bank 2006)

2.1.2 Matrix

The matrix in FRPs is a polymer resin which acts as the binding agent holding the fibers together, redistributing forces in the system, and protecting the fibers from mechanical and environmental damage. The difference between polymer types is based on the functional groups present in the polymer chains and how the chains interact. The two primary functional groups are thermosetting polymers and thermoplastic polymers. A limiting factor for use on many FRP systems is based on the glass transition temperature of the matrix, which is loosely defined as the temperature when a solid begins to soften and become a liquid. For thermosetting polymers, the glass transition temperature is typically around 180^{o} F. It is important for manufacturers as well as engineers to select and employ a matrix with a greater ultimate strain than the fibers. The correct selection ensures the brittle matrix doesn't fail (crack) before the fibers reach their maximum strength capacity (ACI Committee 440).

Typical matrix types in structural engineering applications include unsaturated polyester, epoxy, vinyl ester, phenolic, and polyurethane resins. Unsaturated polyester resins are widely used in the pultrusion process. Epoxy resins are most commonly used for retrofitting of structures because of their good adhesive properties, low shrinkage during curing, and resistance to environmental degradation. Vinyl ester resins are primarily used in the pultrusion production of FRP rebars, and are a combination of unsaturated polyester and epoxy resins.

2.1.3 FRP Composite Properties

AFRP, CFRP, and GFRP are the most widely used FRP systems because they have high ultimate strengths, low ultimate elongations, low thermal conductivity, high chemical resistance, and are light weight. With this being said, it is worth noting the FRP is only as strong or resilient as its components. Since FRPs are composites, they have the combined mechanical and chemical properties of the fibers and matrix. Figure 2.3 shows the tensile stress-strain relationship of a typical FRP and its components. Mild steel does perform better at lower strains than GFRP; however, CFRP out-performs all shown systems. It should also be noted when unidirectional FRP systems are loaded in direct tension they remain linear-elastic (no yielding) until sudden rupture.

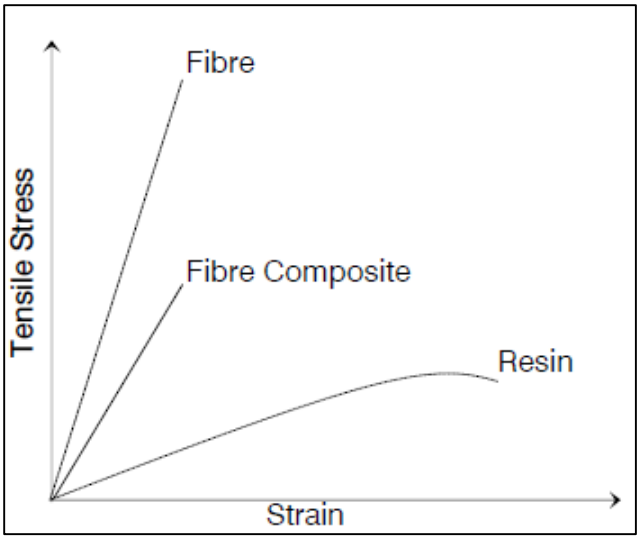

Figure 2.3 Tensile stress-strain relationship for a typical FRP and its fiber and matrix components (Badawi, 2007)

Despite having higher tensile strength properties than steel reinforcement, the compressive strength of FRPs are quite low relative to their tensile strength. For this reason, ACI Committee 440 does not recommend the use of FRP systems in compressive strengthening applications. When FRP is applied to compressive members, it is normally used in such a way as to take advantage of its tensile strength such as confining a compression member, limiting effects like buckling, as opposed to directly resisting compression (Banks 2006).

2.1.4 FRP System Applications

Structural engineers designing repairs using FRP are limited to using externally bonded FRP systems because often only the surface is accessible. Generally, three externally bonded FRP systems are recognized: wet layup, precured, and near-surface mount (NSM) systems. Despite the nomenclature, NSM systems are still classified as an externally bonded FRP system by ACI Committee 440. Selection of externally bonded FRP systems depends on the availability of the product and trained application personnel, the ease and simplicity of application, and, most importantly, the condition and needs of the structure.

Wet layup FRP systems are often used on structures where the application surface is relatively smooth but has an abrupt or curved geometry as shown in Figure 2.4. The smooth surface is a requirement of this system as to ensure proper bonding of the FRP to the structure substrate so an ideal composite action can take place. The wet layup system consists of either a unidirectional or bidirectional fabric, and a polymer resin. In the case of a wet layup system the resin used acts not only as the composite matrix but also as the adhesive securing the FRP to the structure. The fabric is saturated with the resin in the field by hand and then applied and allowed to cure on the structural surface.

Figure 2.4 CFRP fabric sheet wet layup application to girder (CPS Construction Group 2011)

Precured FRP systems are often used when the surface of the structure is smooth and flat, or when it is not practical to use a wet layup. The system consists of either precured (fiber and matrix already combined) unidirectional or bidirectional laminate strips or sheets, typically delivered to the field in thin ribbon strips coiled on a roll. The system requires an adhesive for attaching the system to the structure.

Near surface mount FRP systems are limited to use in RC beam structures because it requires cutting a groove into the soffit of the structure, which then has an FRP rod bonded into it. The FRP bars are typically rectangular or circular in cross-section manufactured using the pultrusion process. While additional time and effort is required cutting the groove, increased flexural properties have been found when the NSM rods are pretensioned (Badawi, 2007).

2.2 Fatigue and Fracture Mechanics

For years, structural engineers have been aware of the fact that cyclic loading of bridges caused by passing traffic can lead to fatigue failure of structural members. Fatigue is caused by cyclic stress ranges, which are below the material's ultimate strength, causing initial microscopic flaws in the material to accumulate and grow. When these small cracks combine into large enough cracks, the cross-sectional area of the member is effectively decreased. If the crack propagates enough, to the point where the applied load causes stress greater than the remaining intact cross-section can endure, a sudden fracture of the member occurs. While fatigue occurs in every material subjected to cyclic loading, in the current study the focus will be on the steel reinforcing bars, which have been shown to be the limiting fatigue component in RC bridge structures (Kim and Heffernan 2008). The steel reinforcement is considered the limiting fatigue component because concrete experiences fatigue cracking at far fewer cycles and has a lower fracture toughness (Dowling, 1999). Additionally, RC beam structures continue to perform to the desired levels despite cracking along the tension face due to the small amount of tensile strength supplied by the concrete in comparison with the rebar. However, when the available tensile strength provided by the rebars is removed from the equation as a result of fatigue induced fracture, the structure cannot endure with just the strength provided by the concrete.

2.2.1 Fatigue Failure Stages

Fatigue failures have three stages: crack initiation, crack propagation, and sudden fracture. While on the macro scale, steel is considered isotropic; at a micro scale it is quite anisotropic with different crystal grains present. For ductile metals, like those composing steel reinforcing bars, the crystal grains are

orientated in a fashion in which slip bands easily occur at the grain boundaries due to the applied stress. As the applied stress is cycled, these slip bands extend leading to initiation of a crack (Barsom and Rolfe 1999). These cracks initiate quicker at locations where stress concentrations are present. Stress concentrations can appear in many different forms, especially in welded components; however, for fully intact straight deformed steel reinforcing bars, stress concentrations naturally occur at the intersection of the transverse and longitudinal ribs as shown in Figure 2.5.

Figure 2.5 Fatigue crack in rebar with initiation at intersection of longitudinal and transverse ribs. (Derkowski 2006)

Once a crack is formed, it propagates perpendicular to the applied stress; in the case of tensile rebar in flexural members, the cracks propagate transversely due to the tensile forces developed. The crack will continue to propagate as long as the stress intensity factor range is above the threshold value (Barsom and Rolfe 1999). The cracked cross-section of a piece of rebar will appear smooth due to the rubbing of the crack faces as the crack opens and closes under cyclic loading. The progress of crack propagation can also be indicated by beach marks extending away from where the crack initiated. Beach marks are semielliptical rings left in the material due to the progressing crack tip as shown in Figure 2.7.

After the crack propagates a sufficient degree, the cross-section of the component is effectively decreased to the point where the applied load induces a stress no longer below the ultimate strength of the material, and fracture occurs. The fracture stage of fatigue failure frequently occurs with no warning. In contrast to the smooth surface produced by crack propagation, the fracture surface is rough as shown in Figure 2.6.

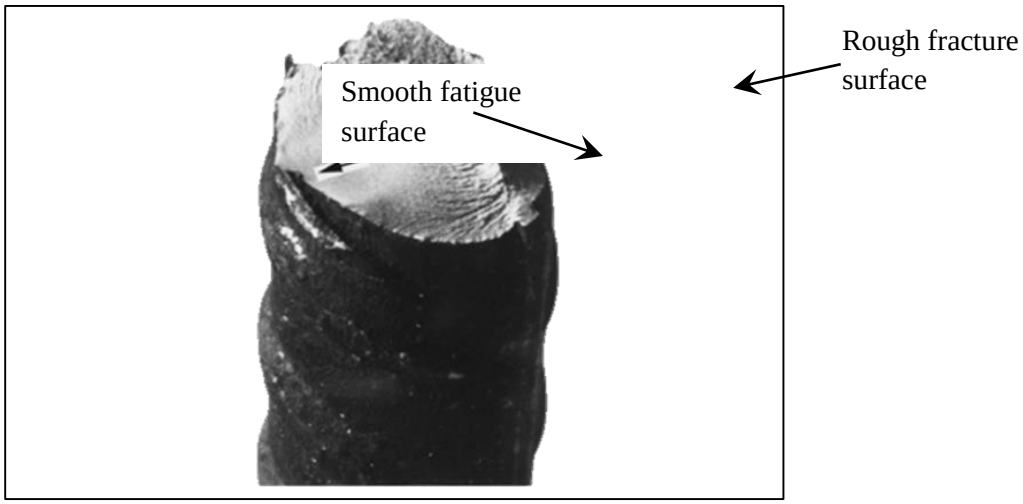

Figure 2.6 Fatigue failure of a steel reinforcing bar with crack initiating from a sharp identification mark (Zheng & Abel 1998)

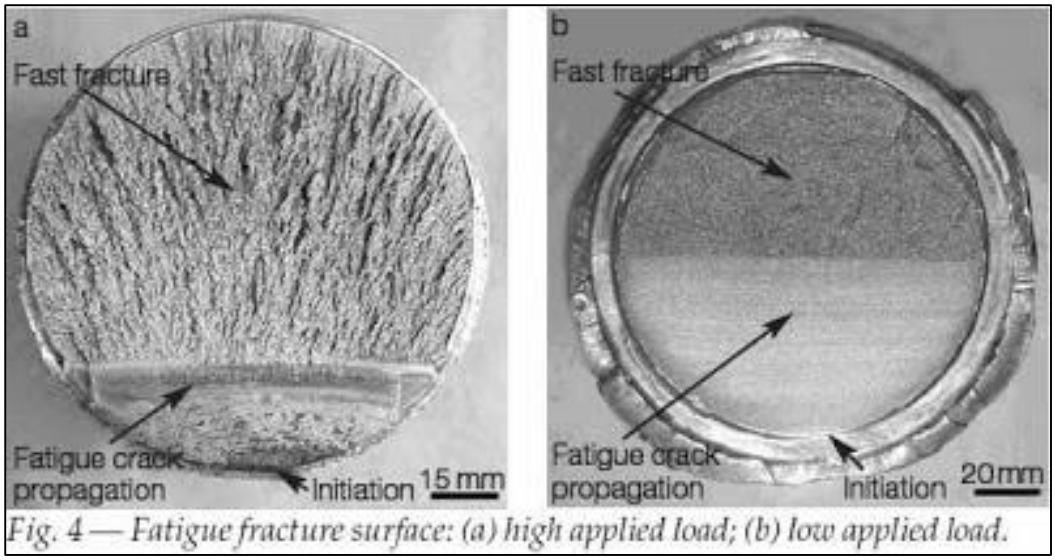

Fig. 4 — Fatigue fracture surface: (a) high applied load; (b) low applied load.

Figure 2.7 Fatigue Fracture of bolts with beach marks visible in fatigue region (Milan et al. 2004)

2.2.2 Linear Elastic Fracture Mechanics

Linear Elastic Fracture Mechanics (LEFM) has been recognized as the primary approach for fatigue and fracture assessment of structures (Barsom and Rolfe 1999). The use of fracture mechanics requires the determination of the material's fracture toughness, nominal stress range, flaw size, and geometry. The stress field near the tip of a crack, in Mode I – opening mode, is characterized by the stress intensity factor, K_I, having units of MPa$\sqrt{m}$. This factor takes into account the nominal stress, σ, crack size, *a*, among other factors, *F*. In its most general form, the stress intensity factor under Mode I loading (opening mode) can be calculated using the following equation:

Equation 1. Stress intensity factor

$$K_I = F\sigma\sqrt{\pi a}$$

Equations have been developed to describe the crack correction factor for many different applications. As for the case of a steel reinforcing bar with a surface flaw, the crack can be described by the equation for a round bar with a semi-circular edge crack.

Equation 2. Crack correction factor for a round bar with a semi-circular edge crack (BS 7910)

$$F = \frac{\frac{1.84}{\pi}\left[\frac{\tan\left(\frac{\pi a}{4r}\right)}{\left(\frac{\pi a}{4r}\right)}\right]^{0.5}}{\cos\frac{\pi a}{4r}}\left\{0.752 + 2.02\frac{\pi a}{4r} + 0.37\left[1 - \sin\left(\frac{\pi a}{4r}\right)\right]^3\right\}$$

Where *a* is the flaw/crack depth and *r* is the radius of the bar.

When the stress intensity factor for Mode I reaches its critical value, K_{IC}, the crack size has reached its critical length and the remaining material can no longer take the applied stress, resulting in fracture. Since this is the stress intensity factor at which fracture occurs, K_{IC} is often referred to as the fracture toughness

of the material. Values for K_{IC} can be determined from material tests such as the Charpy V-notch test, ASTM E23 (2007), or from assessing Equation 1 for the maximum stress a component will experience and the critical flaw length, a_c.

Equation 3. Fracture toughness. Derived from stress intensity factor equation

$$K_{IC} = F\sigma_{max}\sqrt{\pi a_c}$$

In fatigue, when the crack tip is cyclically stressed, this driving force parameter becomes ΔK_I, where the nominal stress term becomes the nominal stress range, $\Delta\sigma$, which is equal to the maximum stress minus the minimum stress.

Equation 4. Stress intensity factor range

$$\Delta K_I = F\Delta\sigma\sqrt{\pi a}$$

Just as a material with a flaw has a critical value for K_I, it too has a threshold value designated as ΔK_{th} for which a fatigue crack will not propagate. Conservative estimates of this threshold value can be determined from the following equation.

Equation 5. Threshold stress intensity factor range

$$\Delta K_{th} = 7(1 - 0.85R) \quad MPa\sqrt{m}$$

In Equation 5 the parameter *R* is the stress ratio, which is equal to the minimum stress divided by the maximum stress (Dowling 1999).

Equation 3 can be rearranged to determine the critical crack length, a_c, if the fracture toughness is determined using a material property test, such as the aforementioned Charpy V-notch test.

Equation 6. Critical crack length

$$a_c = \frac{1}{\pi}\left(\frac{K_{IC}}{F * \sigma_{max}}\right)^2$$

In Equation 6, σ_{max} is the maximum nominal stress in a component.

In order to determine how long it will take a crack, once detected, to reach its critical length, it is useful to determine the crack propagation rate. The fatigue crack growth rate is essentially the increase in crack length (a) per cycle (N) resulting in the ratio (Da/DN). However, since the change in length per cycle is small, the growth rate can be considered as the derivative, da/dN (Dowling 1999).

In 1964 Paris proposed the Paris Law, which correlates the crack propagation rate, da/dN, and the stress intensity factor (Paris 1964).

Equation 7. Paris Law equation

$$\frac{da}{dN} = C\Delta K^m$$

Where *N* is the number of fatigue cycles corresponding to stable crack growth, and *C* and *m* are material constants. The material constant, *m*, is a measure of the sensitivity of the growth rate to stress, and is found from the slope of the linear portion on the log-log plot. The material constant, *C*, is then the y-intercept of the linear portion of the plot (Dowling 1999). The relation between the crack propagation rate and the stress intensity factor range is made up of three regions: threshold region, steady growth, and unstable growth/fracture as shown in Figure 2.8. It should be noted the Paris Law only accounts for crack growth and not initiation, which differs from the more traditional nominal stress range vs. elapsed fatigue cycles to failure, S-N curves, which will be discussed in the next section.

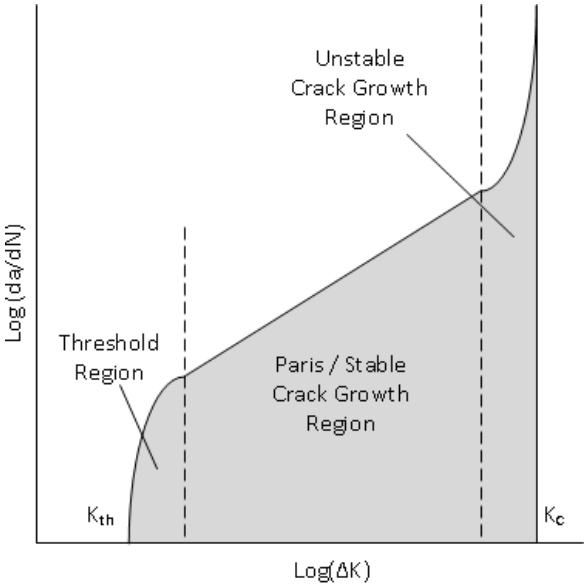

Figure 2.8 Typical crack growth rate vs. stress intensity factor range

Due to the nature of a growing crack in metallic components, the log(da/dN) vs log (ΔK) plot has a distinct S-curve shape. When a small flaw is stressed such that the stress intensity factor range is just above the threshold value, crack growth is initially quite rapid, with the curve generally having a steep slope approaching a vertical asymptote at the threshold stress intensity factor range. (Dowling, 1999). Again, this threshold value is generally the value at which cracks typically won't propagate. The next segment is the stable crack growth region described by the Paris Law. On a log-log plot, this segment should be fairly linear with the crack growth rate and stress intensity factor range increasing at the same rate. The growth rate again accelerates unstably as the stress intensity factor range becomes large, typically as the crack reaches its critical length and fracture occurs.

In addition to the crack growth rate depending on the stress intensity factor range, the growth rate also depends on the stress ratio, R ($\sigma_{min}/\sigma_{max}$), as shown in Figure 2.9. An increase in the stress ratio will cause the growth rate to increase. However, if testing conditions, such as the R value, environment, and testing frequency, are held constant the growth rate will only depend on the stress intensity factor range, ΔK. This is because ΔK accounts for the combined effects of cyclic loading, geometry, and crack length. Therefore, all da/dN vs. ΔK data will fall along a single line on a log-log plot as shown in Figure 2.9.

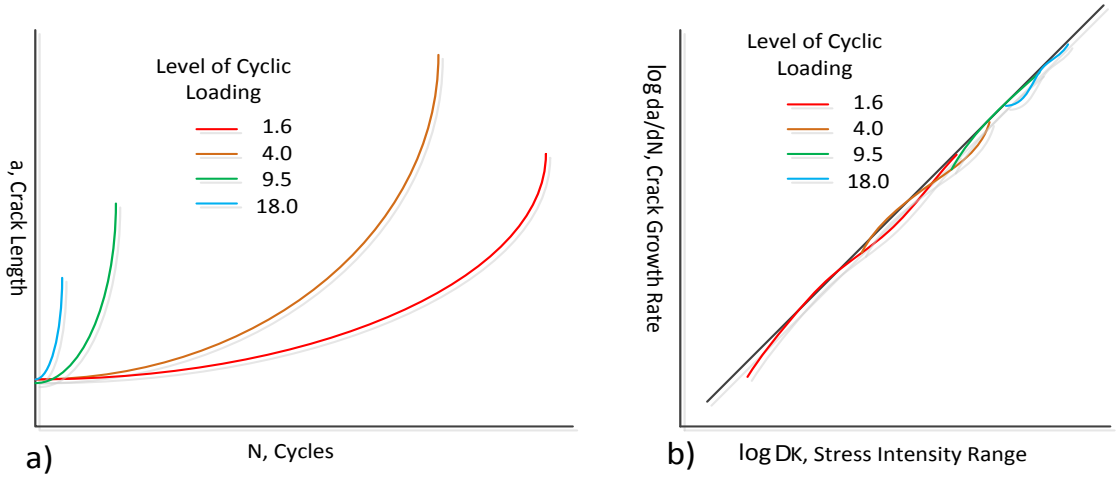

Figure 2.9 a) Crack length vs. cycles data at differing levels of cyclic load applied, b) log da/dN vs. log ΔK data plotted from data in plot a). (Produced from Dowling 1999).

2.2.3 Fatigue Life Prediction and S-N Curves

The use of the Paris Law and knowledge of the factors affecting it (ΔK and R) can effectively be used to determine the fatigue life and safety inspection intervals of an in-service component. According to Dowling (1999) the first step is to test a specimen with a convenient geometry in such a manner as to replicate the fatigue loading in the field at different stress levels, so a range of fatigue crack growth rates are acquired. The derivatives of these fatigue crack growth rates can then be plotted versus the stress intensity factor ranges on a log-log plot in order to create a plot similar to the one shown in Figure 2.9 b). As mentioned in the previous section, the Paris Law material constants can be determined from this plot, which with the stress intensity factor range will produce the crack growth rate. The crack growth rate, however, isn't useful in itself without being able to determine the fatigue life of the component of for which it was determined. The Paris Law, Equation 7, can be rewritten so the number of fatigue cycles from an initial crack length to the critical crack length can be determined. In order to do this, an integration procedure must be utilized solving for N (Derkowski, 2006).

Equation 8. Integration of Paris Law Equation to solve for N

$$\int_{N_i}^{N_f} dN = N_{if} = \int_{a_i}^{a_f} \frac{da}{f(\Delta K, R)}$$

N_{if} is the number of fatigue cycles from the initial cycle to the final cycle. If it is reasonable to assume the crack shape factor, F, is constant or approximately constant throughout the fatigue life due to the crack being relatively small and the effects of R are included in the material constant, *C*, it is possible to determine the fatigue life by substituting Equation 4 into Equation 8.

$$N_{if} = \int_{a_i}^{a_f} \frac{da}{C(\Delta K)^m} = \int_{a_i}^{a_f} \frac{da}{C\left(F\Delta\sigma\sqrt{\pi a}\right)^m} = \int_{a_i}^{a_f} \frac{1}{C\left(F\Delta\sigma\sqrt{\pi}\right)^m} \frac{da}{a^{\frac{m}{2}}}$$

Equation 9. Number of fatigue cycles to unstable crack growth. Derived from Paris Law

$$N = \frac{2(a_c^{\frac{2-m}{2}} - a_i^{\frac{2-m}{2}})}{(2-m)C\left(F\Delta\sigma\sqrt{\pi}\right)^m}$$

Another method for predicting the fatigue life of a component is using stress range-number of cycles, S-N, curves. These curves are constructed by testing numerous specimens at different stress ranges and determining the number of cycles it takes to fail the specimen. By varying the stress amplitude, the number of cycles to failure also varies allowing different points on the curve to be plotted, the higher the stress amplitude the fewer cycles it takes to reach failure, and vise-versa. Eventually, the stress range will be so low that the stress intensity factor will be below the threshold value and the specimen will not fatigue. AASHTO (2012) has set fatigue categories, A-E, B' and E' for various components, which are subjected to fatigue loading. Use of these categories allows an engineer to determine the lower bound fatigue life of a component if he/she knows the stress range in that component. A typical S-N plot is shown in Figure 2.10 along with the AASHTO fatigue categories.

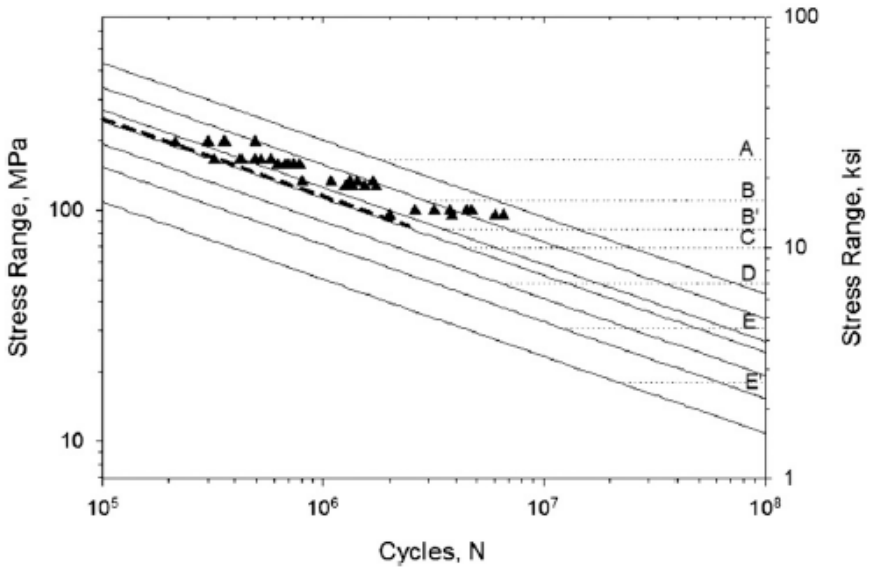

Figure 2.10 S-N test data (Fisher et al. 1974) and AASHTO fatigue design curves

S-N curves are useful due to their simplicity, but in order to determine a fatigue category for a new component many test specimens are needed; this becomes expensive and very time consuming since many fatigue tests reach millions of cycles. In addition, S-N curves don't take into account initial flaw sizes or pre-damage to components, limiting their use and accuracy as a fatigue life prediction method.

2.3 Existing Studies on Fatigue Performance of RC Beams Repaired with FRP

Over the past decade, research on fatigue characteristics of reinforced concrete beams strengthened with FRP has grown rapidly, with many researchers conducting experimental tests. While a large portion of the research has focused on the application of externally bonded CFRP sheets or plates, other FRP types and strengthening systems such as NSM rods have been researched. Most papers concerned with the fatigue behavior of strengthened RC beams address at least one the following topics: 1) different CFRP strengthening configurations, 2) different anchorage systems, 3) impact of environmental conditions, or 4) fatigue life prediction models.

2.3.1 Review Papers

In the literature currently available, two review papers covering the fatigue performance of externally strengthened FRP beams, Kim and Heffernan (2008) and Oudah and El-Hacha (2012), exist with the purpose of informing researchers on the current state of research and the existing codes and design guidelines available to practicing engineers. Both of these papers address fatigue characteristics of the constituent materials, fatigue provisions in design codes such as AASHTO and ACI 440, and fatigue behavior and failure modes of strengthened beams. In addition, both papers present tables summarizing the experimental testing programs for at least a dozen papers on the subject. Oudah and El-Hacha focus more on the available fatigue life prediction models and the fatigue behavior of the materials, whereas Kim and Heffernan emphasize research on debonding and anchorage issues and design considerations.

Both papers summarize the general findings from previous research on the fatigue performance of externally bonded FRP reinforced concrete beams as:

1. The addition of FRP increased the fatigue life.
2. Fracture of the tensile steel reinforcement was the initiating failure mode.
3. The critical parameter was the stress range in the reinforcing steel.
4. Debonding in the FRP-concrete interface needs to be addressed in order to achieve better performance from the repair.

Oudah and El-Hacha noted the fatigue response followed a bilinear trend as a result of reaching the full cracking stage early on during cycling. Kim and Heffernan pointed out pre-damage to the beam had a significant effect on the fatigue behavior, therefore must be accounted for in repair designs.

The authors finished their respective papers with research needs. The emphasis of the two sections was on developing design charts or procedures for practicing engineers, especially for cases where the application of such FRP systems will be for pre-damaged, retrofitted structures. The researchers found that the current design codes, AASHTO, ACI440, and ACI 215, only provide guidelines on the stress range and don't take into account other factors which can affect the fatigue life. Kim and Heffernan explicitly state, "Detailed design guidelines for the fatigue limit state for reinforced concrete beams externally strengthened with FRP should be developed. Current design guidelines merely limit the strains and stresses in the FRP without providing detailed information such as the level of predamage in concrete or steel, environmental conditions, applied loading ranges, or expected fatigue lives." Thus it was the goal of this study to develop a design procedure based on a fatigue limit state for the repair of pre-damaged RC bridge girders with externally bonded FRP.

2.3.2 FRP Strengthening Configurations

Most studies considering the fatigue performance of RC beams repaired with FRP have shown an increase in fatigue life with the addition of FRP; however, Kim and Heffernan (2008) reported the degree of fatigue life extension varies greatly, with many factors affecting the fatigue performance. Barnes and Mays (1999), Shahawy and Beitelman (1999), Mosoud et al. (2001), Papakonstantinou et al. (2001), El-Hacha et al. (2003), Aidoo et al. (2004), Heffernan and Erki (2004), Gussenhoven and Brena (2005), and Toutanji et al. (2006) showed that fatigue failure of RC beams strengthened with FRP was initiated by fatigue-fracture of the tensile reinforcing bars followed by concrete crushing, FRP delamination, and/or fracture of the FRP. The fact that so many studies have found the tensile steel reinforcement to be the limiting fatigue component allows future studies to focus on the fatigue behavior of this element. Gussenhoven and Breña (2005), Aidoo et al. (2006), Al-Rousan and Issa (2011), Shahawy and Beitelman (1999), and Heffernan and Erki (2004) investigated different configurations of externally bonded CFRP, including number of plies, width of plies, and externally bonded prepreg strips versus hand laid-up sheets. Gussenhoven and Breña's testing was unique in the fact the 13 tested beams were the smallest of any found in the open literature, measuring only 914 mm in length. The variations in the CFRP laminate configuration and testing consisted of fatigue testing five beams strengthened with a single ply, 89-mm-wide sheet of M-Brace C-130, three beams that had a single, 51-mm-wide ply, two beams that had two plies of the 51-mm-wide laminate, and three beams that were cyclically loaded 500,000 times in an unstrengthened state at 50% of the steel yield strength, then strengthened with a single layer of 51-mm-wide laminate and cycled until failure. Results found greater laminate thickness delayed fatigue failure of the reinforcing steel. The most astounding finding of the study was increased number of cycles to failure of beams with pre-damage. This result gives the indication CFRP application does not extend the fatigue life of RC beams, which is contrary to the findings of every other study found. Kim et al. (2008) suggested the reason for these results was due to the same stress range being applied to the steel reinforcement whether the beam was strengthened or not and due to the small size of the test specimens. General findings from the other studies include:

- NSM exhibited greater ductility than externally bonded FRP sheets due to improved bond characteristics (Kim and Heffernan 2008) (Badawi 2007).
- Increased number of FRP layers and concrete contact area resulted in a decrease in mid-span deflection and an increase in stiffness, ultimate load capacity, and fatigue life. (Kim and Heffernan 2008) (Aidoo et al., 2004) (Al-Rousan and Issa 2011)
- Strengthening of the sides of beams resulted in increased effectiveness of repairs as it limited width and propagation of shear cracks and provided confining forces in the beam. (Al-Rousan and Issa 2011) (Masoud et al. 2005) (Shahawy and Beitelman 1999)

2.3.3 Corrosion Effects

Newly constructed RC structures can generally be considered quite impervious to environmental attack as the concrete provides a highly alkaline environment around the steel reinforcement, which resists corroding (Masoud et al. 2005). However, after many years in service, RC structures are prone to cracking of the concrete, which can progressively get worse if the structures experience freeze-thaw cycles or overloading caused by heavy trucks. If these cracks reach the steel reinforcement, chloride attacks from deicing agents or salt water will eliminate the passive alkaline film and the steel will begin to corrode. The effect a corrosive environment has on an RC structure is twofold: first, the formation of rust will cause cracks to widen and concrete to spall-off, further exacerbating the problem; second, the corrosion will reduce the steel reinforcement cross-sectional area and produce corrosion pitting. In regard to fatigue, both the reduction in cross-sectional area and corrosion pits can greatly decrease the fatigue life (Masoud et al. 2005). With a reduced cross-section, the remaining intact steel will experience an increased nominal stress thereby increasing the stress intensity at any flaw, which due to the formation of corrosion pits, there are many. The issue then becomes can FRP repairs of these structures reduce the

steel stress range such that fatigue cracking stop or at least slows such that fracture never occurs within the service life.

Masoud et al. (2005) investigated the fatigue performance of RC beams that were lab corroded and repaired with GFRP sheets. It was found that reinforcing bar pit corrosion reduced the fatigue life significantly, up to 78% of an uncorroded control specimen, and even when the reinforcement was corroded to a minor degree (5% mass loss), corrosion pits were observed to have formed as shown in Figure 2.11. Since FRP repairs can be implemented in order to add strength to a member with a severe degree of corrosion loss; in order to make up for the reduced cross-sectional area, the presence of corrosion pitting needs to be taken into account when looking at the fatigue life of the member.

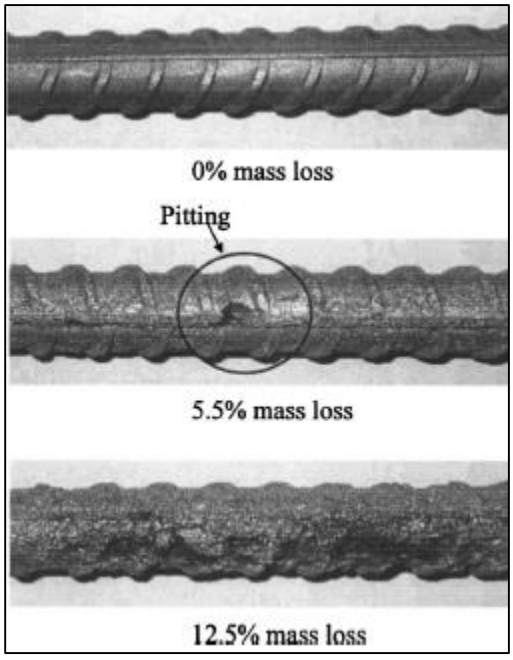

Figure 2.11 Corrosion pitting shown for varying degrees of corrosion (Masoud et al., 2005)

The study by Gonzalez et al. (1995) sought to obtain values for maximum corrosion pit depths developed in steel rebars embedded in concrete. It was proposed the maximum pit depth could be estimated using the following equation.

Equation 10. Maximum corrosion pit depth

$$P_{max} = I_{corr} \times t \times R$$

where P_{max} is the maximum pit depth in mm, I_{corr} is the corrosion current density in μA/cm^2, t is the time in years , R is the ratio of P_{max} to P_{avg}. The authors found I_{corr} values to range from 0.001-0.005, 0.005-0.01, and >0.01 for low, medium, and high corrosion levels, respectively. R values were found to range from 4-10 with higher values correlating to more localized pitting. After six years in the Barcelona, Spain, environment, P_{max} values were found to range from 1.1 – 5.5 mm and R values were found to range from 2.7 – 8.9.

2.3.4 Life Prediction Models

Studies performed by Dong et al. (2008), and Gordon and Cheng (2011) sought to develop equations and methods for characterizing fatigue life extension provided by FRP applied to RC beams. Dong et al. (2008) derived the following equation from fatigue testing 10 RC specimens strengthened with externally bonded CFRP

$$\log(N) = 6.905 - 0.0046\sigma_r$$

where N = number of cycles to failure; and σ_r = applied steel stress range(MPa). The correlation factor was found to be 0.8808. Gordon and Cheng (2011) summarized existing S-N prediction models and derived models from available literature data. Each model's percent accuracy was determined by comparing its predicted result with the experimental results of all other studies. Although some of the S-N models provided fatigue life prediction accuracies within 10% of the experimental value for a particular study's data set, high inaccuracies over multiple sets of data limited any one model from providing a solid fatigue life prediction.

A 1979 study by Lovegrove, Salah El Din, and Daoud investigated the use of LEFM to predict the fatigue crack growth rate in steel reinforcing bars embedded in concrete. Similar to the current study, the use of the Paris Law was highlighted and the determination of the materials constants *C* and *m* was a major focal point of the study. The authors note the difficulty of continuously measuring the fatigue crack growth throughout testing due to the limitations on having the rebars exposed. In order to overcome this obstacle, the authors propose testing two specimens, each with different initial crack lengths and tested at different stress ranges. Using an integrated form of the Paris Law equation, similar to Equation 8, the authors would have two equations with only two unknowns, the material constants, since all other parameters are known from testing. The authors then experimentally tested four beams with varying initial notch depths all at the same stress range and found *m* to equal 5.3 and *C* to equal 6.3E-20. These values were then compared with values obtained from similar steel fatigued in air, which found *m* to equal 3 and *C* to equal 2.8E-13. The difference in these values suggested the fatigue crack growth rate of steel reinforcing bars embedded in concrete is lower than in air. The authors did note the stress range in the rebars could not be directly measured at the time, therefore the use of conventional linear elastic equations for RC beams was used, which might have had an effect on the determined values. The authors conclude the proposed technique can accurately predict the material constants of the Paris Law.

A study conducted by Rocha and Brühwiler (2012) also investigated fatigue life prediction using LEFM. The study gave background on LEFM and the Paris Law along with the need equations and well-accepted values so to predict the fatigue life of a RC flexural member. The authors then perform a case study on a railway bridge in Brazil to determine the fatigue life at the current service level as well as under increased use and loading.

The only study found in the open literature applying LEFM to predict fatigue life of RC beams repaired with FRP was performed by Derkowski in 2006. Similar to other studies which used LEFM as the bases for prediction Derkowski also used the Paris Law to determine the number of cycles to failure of the reinforcing steel. The study was unique in several ways: first, the primary goal of the study was to determine a coefficient of FRP strip position which when used with the Paris Law would be able to more accurately predict the fatigue life of a reinforcing bar within the influence area of an externally bonded FRP strip. The proposed model takes into account the energy absorbed by the strengthening and how this effects the stress intensity factor term in the Paris Law equation. It is the aspect of using the absorbed energy, which is the second unique aspect of the study. Derkowski relates the absorbed energy to the J-integral, and then with the modulus of elasticity of the steel, to the stress intensity factor range. The

proposed model was then validated with fatigue testing four RC beams with different CFRP strip configurations and comparing the experimental fatigue life with the obtained using the process described. The results showed the typical increase in fatigue performance with addition of FRP; however, the most important finding was the positive agreement between the predicted and experimental fatigue lives, which at the worst had a difference of 21.5%.

As mentioned previously, due to the empirical nature of S-N curves, the application of these models for predicting fatigue life of strengthened RC beams is often inaccurate due to testing and specimen variation. For that reason and the fact that the use of LEFM can take into account more of the factors that affect the fatigue life, such as pre-damage, and the promising results of recent studies, for the present study the use of LEFM was decided.

2.3.5 Other Testing Variations

Heffernan and Erki (2004), Papakonstantinou et al. (2001), Toutanji et al. (2006), Gussenhoven and Breña (2005), Aidoo et al. (2006) and Barnes and Mays (1999) considered the effect load intensity had on the fatigue performance of RC beams strengthened with FRP; either adjusting the loading as a percentage of the steel yield strength or a percentage of the static capacity of the unstrengthened beam. It was generally found that loading between 30% and 50% of the steel yield strength did not produce fatiguing of the specimen; therefore, for the sake of testing practicality, the stress ranges induced in the rebars of the test specimens were much higher than those that would typically be experienced in the field. It was not uncommon for the steel stress ranges in unstrengthened beams to reach 200 MPa with some specimens reaching 400 MPa. These values are 19% and 60% higher, respectively, than the 162 MPa permissible stress range recommended by AASHTO. It will be shown later in this paper that the stress ranges produced in the tensile steel reinforcement of test specimens for the current study were between 88 and 107 MPa, 21% and 26% of the yield strength of the steel reinforcement, which still produced fatigue failure of the rebars.

2.4 Existing Design Guidelines and Recommendations

Currently ACI 440.2 *Guide for the Design and Construction of Externally Bonded FRP Systems for Strengthening Concrete Structures* is the most widely used and recognized design document for FRP repairs of RC structures within the U.S. The design approach taken by ACI 440.2 for serviceability of a flexural member limits the stress in the steel reinforcement to below 80% of the yield strength to avoid inelastic deformations; no other limits are placed on the stress in the steel. Fatigue failure of the FRP is addressed by limiting the sustained plus cyclic stress in the different FRP types as a function of the ultimate tensile design strength. While the provision states, "the possible failure modes and subsequent strains and stresses in each material should be assessed," at no point is fatigue of the steel reinforcement considered. Therefore, in order to address fatigue of the steel reinforcement, which has been shown to be the primary failure mode, other design codes such as AASHTO LFRD Bridge Design Specification or ACI-215 must be used.

Section 5: Concrete Structures of the AASHTO Bridge Design Specifications states the following fatigue consideration for steel rebars shall be met:

Equation 11. Load-induced fatigue design criteria (AASHTO)

$$\gamma(\Delta f) \leq (\Delta F)_{TH}$$

where γ = the load factor for the Fatigue I load combination, Δf = the live load stress range due to the passage of the fatigue load (MPa), and ΔF_{TH} = constant-amplitude fatigue threshold, which is equal to 165 - $0.33f_{min}$ for straight reinforcement, where f_{min} is the minimum live-load stress (MPa) resulting from the Fatigue I load combination, combined with the more severe stress from either the permanent loads or the permanent loads, shrinkage, and creep-induced external loads. While AASHTO does more to provide limits on the steel reinforcement stress range, because it is for new construction, it is concerned with preventing crack initiation and does not address fatigue damage accumulation.

ACI-215 *Considerations for Design of Concrete Structures Subjected to Fatigue Loading* recommends for straight deformed steel reinforcement in non-prestressed members, the stress range shall not exceed the value computed from the following expression:

Equation 12. Recommended stress range limit for non-prestressed straight deformed reinforcement (ACI-215R)

$$S_r = 161 - 0.33\ S_{min}$$

where S_r = stress range (MPa) and S_{min} = algebraic minimum stress (MPa). The similarity between the limits set by AASHTO and ACI-215 should be noted. While ACI-215 does discuss other variables affecting the fatigue performance such as minimum stress, bar size and type, geometry of deformations, yield strength, and bending, no recommendations on fatigue life are made based on these variables.

The currently available design codes simply limit the stress range to a level below the fatigue threshold, with no consideration as to how long the FRP repair will extend the fatigue life at the current live load stress range or any other variables affecting the performance. In other words, the current design philosophy essentially recommends the engineer design an FRP repair scheme that produces an overly conservative, infinite fatigue life.

2.5 Measuring Fatigue Crack Growth

In order to obtain valid results of the crack growth rate within the rebar cross-section, an accurate method of measuring the crack length was needed. The trouble with measuring crack propagation in the rebar of RC structures, compared with entirely steel structures, is rebar generally cannot be visually inspected during loading due to it being embedded in concrete. Several methods were investigated based on a chart provided by Frost et al. (1974), shown in Figure 2.12 listing fatigue crack growth measurement techniques, including several non-destructive testing (NDT) methods as well as visual methods. While some of the measurement techniques provided by Frost were developed for crack growth measurement in steel components, many appeared to be applicable to the steel in RC components.

Method	Usage	Advantages	Disadvantages
Microscopy techniques	Sheet and plate test-pieces. Photography sometimes used	Cheap. Easy installation.	Difficulty of crack tip location without stroboscopic light. Only surface measurements possible during test. Difficult to automate.
Mechanical methods	Rotating bend test pieces. Sheet, plate, and others depending on displacement gauge used	Use of compliance change which can be measured externally away from specimen.	Restricted to tests where compliance calibration (relationship between specimen stiffness and crack length) is known.
Acoustic methods	Applicable to most types of test-piece	Very small probe required, can be mounted easily; useful in low- and high-temperature tests.	Errors due to background noise and calibration is difficult
Electrical techniques	Continuity gauges usually used on sheet and plate samples, could be used for surface measurements on other test-pieces	Electrical signal gives easy automation.	Difficulty of connecting wire and foil gauges. Gauges must break when crack passes. Only surface measurement.
Eddy currents	Used on surface crack monitoring of sheet test-pieces; others should be possible.	Easily adapted to automatic process. Small probe which is not in contact with test-piece.	Not yet used on thicker samples, may only be useful for surface measurement. Expensive.
Electrical resistance or potential measurement	Used on sheet and plate test-pieces	Easily adapted to automatic process. Only four leads attached to specimen, therefore ideally suited for high- or low-temperature tests	Problems of insulating the test-piece. Initial calibration problem thought to be overcome.
Ultrasonics	Ideally suited to compact fracture toughness test-pieces. (Fig. 5.2).	Easily adapted to automatic process. Internal measurement of crack front.	Expensive compared to other techniques. Measurements restricted to thicker type test-pieces.

Figure 2.12. Fatigue Crack Growth Measurement Techniques (Frost et al, 1974)

NDT methods for determining the fatigue crack growth rate were initially investigated because they would allow crack measurement in an intact RC beam, where direct access to the rebar at the crack location was not possible. NDT is any technique used to evaluate a material, component, or system without causing damage. Several types of NDT commonly used in structural engineering applications include acoustic emission, electro-magnetic, radiography, ultrasonic, x-ray, impact echo, and electric potential. The problem with a lot of these methods is they are limited to determining the location of flaws, voids, joints and depth, and placement of rebar and conduit and are unable to determine propagation of cracks with any certainty. Despite these limitations engineers have been innovative in the use of some of these methods, eventually being able to determine the size, location, and growth rates of fatigue cracks in concrete. While some of these methods are unrealistic for field use, the goal of this study was not to investigate the applicability of such methods for field use but to study how fatigue crack growth rates are affected by the application of CFRP to RC structures.

2.5.1 Acoustic Emission

One NDT method shown to be effective in evaluating the fatigue crack growth rates in two-dimensional members is acoustic emission (AE). The technique involves sensing transient elastic waves, which are generated when energy is rapidly released from a localized source, often a flaw or void, as they propagate through the solid material. The AE method is unique in the way the measured energy signal is supplied from the test material, through the stressing of a flaw, and not from an external transducer.

With technological advances in computing and signal processing, the AE method has become commercially available and capable of detecting the small changes in the stress wave as a result of a growing crack. Shah and Kishen (2012) have shown with proper calibration this method can determine the location of a crack in a material and with continued monitoring determine the crack propagation characteristics under fatigue loading. However, the problem with translating this method to the current study is that the interest of this study is in determining the crack growth rate within the reinforcing bars, which are essentially one-dimensional. The AE method would only be able to identify the location of cracking and not the growth of a fatigue crack because the AE sensors would only have access to the rebars, which would have to be extended out the ends of the beam. Along with a substantial cost and the need for a skilled technician, a more direct and economical method was pursued.

2.5.2 Electric Potential Drop

Another method suggested by Frost for studying the fatigue crack growth characteristics was electric potential drop. This method was initially investigated because it, too, would need physical access to rebars just as the AE method did. The electric potential drop method involves measuring the drop in electric potential energy as the electric resistance of the material increases between the points of measurement.

In general, there exists two different categories of the electric potential drop method: 1) the alternating current technique (ACPD) and 2) the direct current technique (DCPD) (Nordtest Method 1988). In the ACPD technique, an alternating current is passed through the metal, where most of the current density is carried only in a thin layer on the metal's surface due to the skin effect. In order to determine the crack depth, the voltage must be measured, using potential electrodes, across the crack mouth distance both before and during the presence of the crack. The crack depth can then be measured by the following expression:

$$d = \left(\frac{V_c}{V_o} - 1\right) * \left(\frac{s}{2}\right)$$

Where

V_o = measured voltage between the electrodes when no crack is present
V_c = measured voltage between the electrodes with a crack present
s = distance between potential electrodes

Essentially, the ACPD technique involves measuring an increasing current path around the crack tip and relating that increased path with a progressing crack.

The DCPD technique involves passing a direct current through the metal, where the current flows through the entire cross-section, and measuring the voltage across a distance between the applied current. Using Ohm's law the measured voltage will be given by the expression:

$$V = IR = I(\frac{\rho s}{A})$$

where

V = measured voltage
I = applied current
R = electrical resistance
r = material resistivity
s = distance between potential electrodes
A = cross-sectional area

From this expression it can be seen that as a crack grows the cross-sectional area decreases, resulting in an increased resistance. Additionally, if the current is kept constant, the measured voltage must also increase at the same rate as the resistance, allowing an equation for crack depth as a function of voltage to be derived.

The electric potential drop methods do have some limitations, which were eventually determined to be too large to work in the current study. The ACPD method requires the potential electrodes to be placed close to the crack mouth in order for the small changes in the current path to be measured. The DCPD method is largely dependent on the resistivity value of steel, which has a value varying from 1.43-1.71*10^{-7} Wm, making the measured voltages very small. The problem with very small voltage readings is the equipment required to measure the slight variation due to crack growth is very expensive. Additionally, due to the interlocking between the concrete and the reinforcing steel in RC structures, the crack mouth is restricted from opening as far. This restricted movement allows sustained contact between the crack faces, resulting in continued current flow despite the crack tip having passed this region. The increased area for current flow, regardless of electric potential drop technique, results in discrepancies in the measured voltage and therefore crack length.

2.5.3 Microscopy

The physical and economical feasibility of other NDT methods led to the investigation of visual inspection of fatigue cracks. The instrumentation for visual inspection of fatigue cracks is typically some sort of microscope due to the relatively small size of fatigue cracks in steel rebars. The use of microscopy relied upon whether visual inspection of the crack was possible. The tensile rebars in RC flexural members are embedded in concrete so that the tensile stresses can be transferred from the concrete, which is weak in tension, to the rebars, which are strong in tension. Additionally, as mentioned before, the concrete cover provides protection of the rebars from external environmental attacks. However, in the current study rebar protection wasn't needed as the beams would be tested relatively quickly after fabrication. Furthermore, in order to keep the fatigue test of each beam to a reasonable time frame, a relatively high stress loading would need to be applied to the beam. As discussed in further detail in the methodology section of this paper, the loading was calculated to produce an applied moment greater than the cracking moment of the beam, meaning the beam would have flexural crack up to the neutral axis of the beam. Because the concrete below the neutral axis was cracked, it would hardly provide any tensile strength; therefore, it was hypothesized a small portion of concrete could be removed, exposing the rebar for visual inspection via a microscope. A digital microscope was used for practical purposes because it, along with the accompanying software, could measure the crack length directly from the digital photos. In order to validate the prediction that removal of a small portion of the concrete, to allow for visual inspection, would have minimal effect on the overall structural performance of the beam and fatigue crack

growth rate, a small scale test was performed and one of the full scale test beams was fabricated without a void and compared to two identical beam with a void.

2.6 Significance of Present Research

The current study aims to provide more explicit recommendations for design of externally bonded FRP repairs of RC flexural members for fatigue limit states by using fatigue and fracture mechanics, specifically the Paris Law, to specifically consider fatigue performance of the steel reinforcement. This approach is innovative because much of the previous research interested in developing a fatigue life prediction model for FRP repaired beams has focused on the use of S-N curves for the whole beam despite the fact failure of the steel is known to control beam performance. The approach studied here has the potential to be less constrained by specific beam geometry. The experimental portion of the study determined the fatigue crack growth rate of rebar in both strengthened and unstrengthened beams and is believed to be the first test to do so. Furthermore, the study addresses the presence of pre-damage in the form an artificially produced corrosion pit. The current study is also one of only a few studies that have sought to experimentally determine the Paris Law material constants for steel reinforcing bars in RC beams repaired with FRP. The study also addresses the inherent difference between designing an FRP repair for strength and for fatigue, as current code provisions focus on the former, and presents a design process based on a specific fatigue life extension rather than recommending that RC members be strengthened to a level at which fatigue will never occur.

In general, it is hypothesized the current study will be able to predict the crack growth rate and fatigue life extension of RC beams repaired with externally bonded CFRP using LEFM and the proposed visual means of inspection. These results will then allow for the development of a design process for RC beams repaired with CFRP, which has a fatigue limit state.

3. METHODOLOGY

3.1 Small Scale Testing

As described in section 2.5, a visual inspection of the rebar was determined to be the most economical and direct method for measurement of the fatigue crack growth rate. The direct access to the rebar also reduces uncertainty in results that may be present with other NDE techniques. In order to validate the prediction that removal of a small portion of the concrete would have minimal effect on the overall structural performance of the beam and fatigue crack growth rate, a small scale test was performed. The rational for the test was: if the small scale beams with and without rebar access holes have similar performance, then the access holes are not significantly affecting beam performance. Furthermore, the performance in the actual test specimens should also be unaffected by the access holes since the removed concrete makes up a greater portion of the cross-section in the small scale beams.

3.1.1 Manufacturing and Dimensions

Three small scale beams were constructed, each having a span of 864 mm, depth of 89mm, and width of 89 mm as shown in Figure 3.1. The steel reinforcement of each beam consisted of a single 10 mm, Grade 60 (420 MPa), black bar as the tensile reinforcement and shear stirrups bent from smooth steel bar with nominal area of 40.65 mm^2. The tensile reinforcement was placed at a depth of 70 mm below the compression face of the beam. During the fabrication of the stirrups, a surface roughness was applied to achieve interlocking between the concrete and stirrup. The stirrups were tied to the tensile rebar in the shear zone of the beams with 50 mm spacing between them as shown in Figure 3.2. Two of the beams had cylindrical sections of the concrete removed by placing foam tubing in the forms before concrete placement as shown in Figure 3.3. The missing concrete section measured 38 mm deep and traversed the width of the beam. Quickrete high early strength sack concrete, which is rated to achieve a 27.6 MPa compressive strength at 28 days of curing, was also used. A concrete vibrator was used while placing concrete to reduce air voids in the beams. For further identification of each beam the following designations were used: Beam 1 was fabricated with no void in the concrete and had three strain gages, Beam 2 was identical to Beam 1 but with a void, and Beam 3 was identical to Beam 2 but only had the single strain gage.

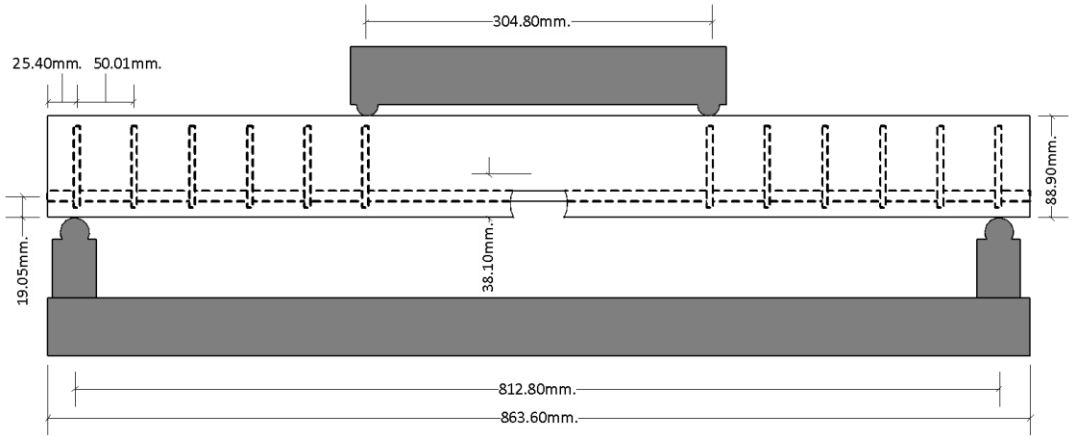

Figure 3.1 Small scale test beam shown with rebar access hole, reinforcement detail, and support and loading points.

Figure 3.2 Shear Stirrups with surface texture shown

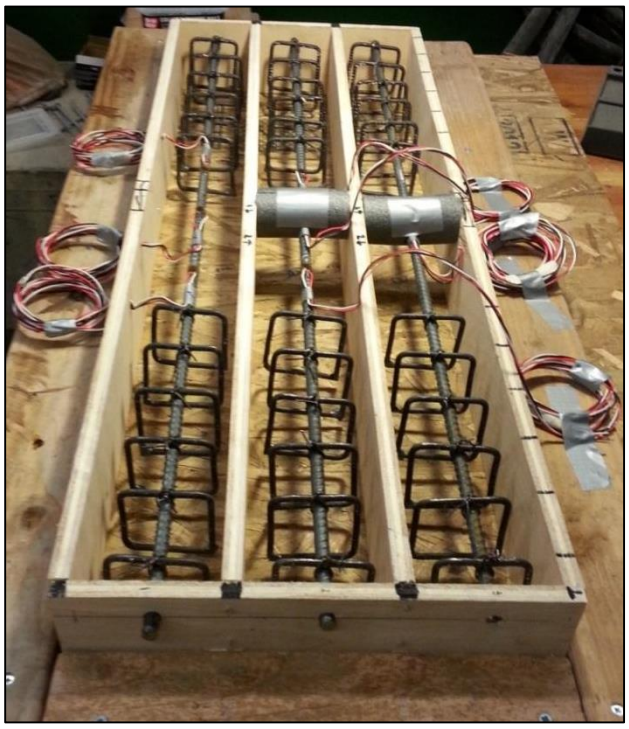

Figure 3.3 Small scale beam forms with foam cylinders for access holes

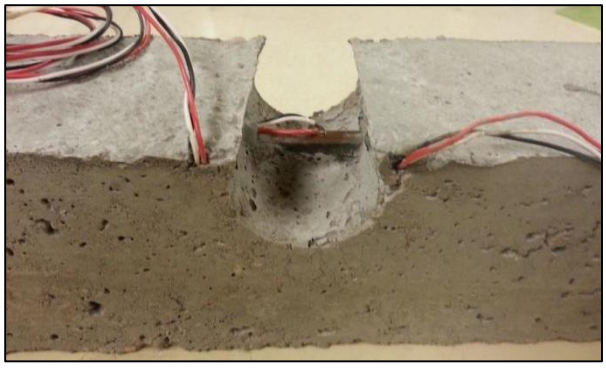

Figure 3.4 Small scale beam with rebar access hole.

3.1.2 Instrumentation

The instrumentation used for the small scale beams consisted of 350 Ω foil backed strain gages attached to the single longitudinal bar. The ribs on the rebar were ground down and the surface smoothed using silicon carbide paper as per the installation instructions of the strain gage manufacturer as seen in Figure 3.5. Prior to concrete placement, lead wires were soldered to the strain gages and a protective coating applied to eliminate damage to the strain gages during concrete placement.

A picture of the strain gage layout on each beam is shown in Figure 3.6.The strain gage layout was used so the tensile stresses developed in the reinforcement could be determined both in and outside of the removed concrete section to ensure the stresses in the beams with and without access holes were acceptably close in value. Theoretically the stresses should be the same, up to yielding of the reinforcement, since the beam was loaded in four point bending and the gages were all in the constant moment region.

Figure 3.5 Deformed steel reinforcement with ribs ground down and sanded

Figure 3.6 Strain gage layout

3.1.3 Testing

The cured beams, shown in Figure 3.7, were tested monotonically to failure under four point bending with the span between loading points being 305mm and the span between supports being 813 mm. Applied force and displacement was measured internally by the United Testing Systems universal testing machine. The strain measurements were made by attaching the strain gage lead wires to a Campbell Scientific CR1000 data logger. In addition to ensuring the stresses in the rebar were similar, the strength and deflection of each beam was determined. Furthermore, the applied force and measured deflection of each beam was used to determine the stiffness variations between beams.

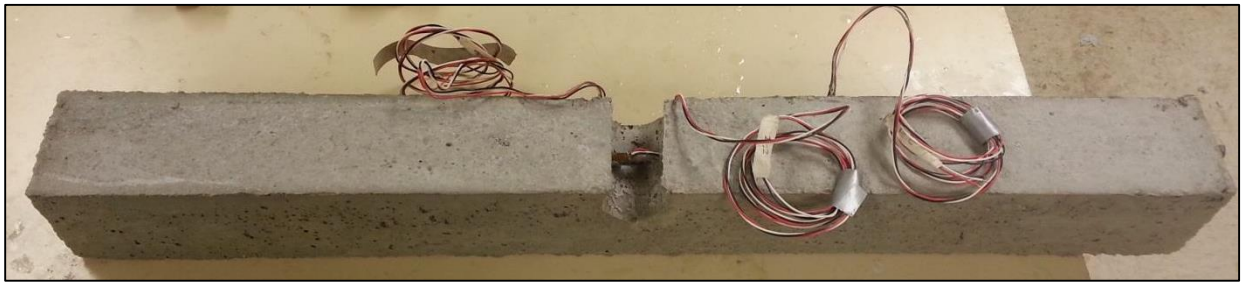

Figure 3.7 Cured small scale beam with access hole and strain gage lead wires shown

3.1.4 Small Scale Results

The test results, Figure 3.8 and Figure 3.9, show all three beams had very similar load-deflection curves with negligible differences in stiffness in the elastic range and comparable strain levels in the rebar prior to overload failure. While the data do show Beam 1 yielding at a lower load level than Beam 2, because the fatigue tests for the full scale beams were to be run well below the level where rebar yielding would occur, this test showed good agreement with thinking the void in the concrete wouldn't affect the fatigue performance of the beams.

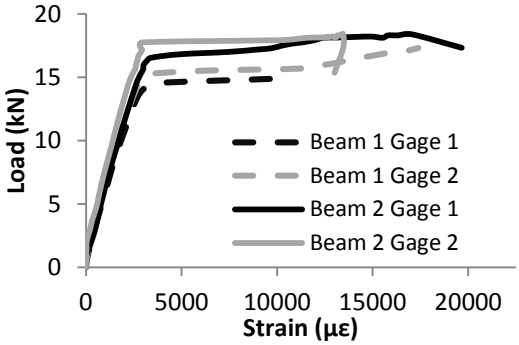

Figure 3.8 Small scale beam load vs. deflection curve

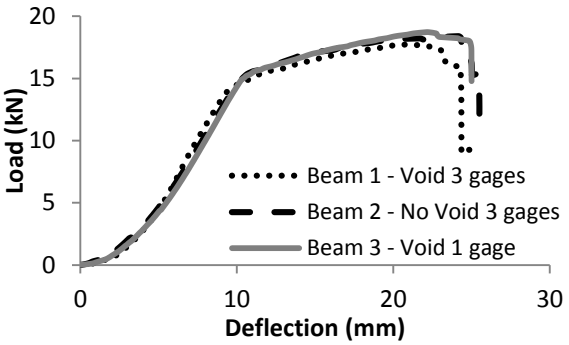

Figure 3.9 Small scale beam load deflection curves

3.2 Full Scale Experimental Test Program

The large scale experimental program consisted of seven beams to be fatigue tested, while a total of ten beams were fabricated, three beams were for a similar project. The beams were divided into three groups in addition to a control beam: a non-CFRP strengthened group, a typical modulus CFRP sheet strengthened group, and a high modulus CFRP strip strengthened group. The following sections detail the design, fabrication, testing set up, and instrumentation layout of the experimental test specimens.

3.2.1 Test Matrix

Seven 4,725-mm-long, 250-mm-wide, and 400-mm-deep steel reinforced concrete beams were constructed for the experimental investigation. The beams were fabricated with two A615M Gr 420 No. 10 compression bars, three A615M Gr 420 No. 19 tension bars, and a total of 18 A615M Gr 420 No. 10 shear stirrups as shown in Figure 22. The stirrups were spaced at 170 mm within the shear spans of each beam. Additionally, each beam's outermost tensile rebars were notched to promote fatigue crack growth from this point; this is discussed further in the following sections. Through the remainder of the paper the following designations will be used for each full scale specimen:

Beam 1: No rebar access void in the concrete, no externally bonded CFRP
Beam 2 and 3: Rebar access void at mid-span, no externally bonded CFRP
Beam 4 and 5: Rebar access void at mid-span, externally bonded common modulus CFRP sheet
Beam 6 and 7: Rebar access void at mid-span, externally bonded high modulus CFRP procured strip

The test matrix was designed in order to achieve the stated objectives using the proposed methods given in the Introduction section. Beams 1, 2, and 3 were designed in order to verify the results obtained from the small scale testing on the effect the rebar access void had on the overall beam performance, and on the fatigue performance of the steel reinforcement. Comparisons between the crack growth rates of groups 2, 3, and 4 would allow for determination of the how much extension in fatigue life each repair provides as well as the values for the Paris Law material constants. Comparison between the fatigue performance between groups 3 and 4 would provide answers on whether there is a difference in designing an FRP repair in order to solely add strength or if there is a correlation between increased strength and extended fatigue life.

All beams were fatigue tested under four-point loading using a single servo-hydraulic actuator applying a sine waveform under force control at a frequency of 2.5 Hz. It was initially predicted a 60 kN - 110 kN loading would produce a stress range in the reinforcement, which would allow crack propagation and limit the fatigue life to a reasonable number of cycles. However, after running Beam 1 at this loading

level for 700,000 cycles with no signs of fatigue, it was determined that the stress range needed to be larger. Therefore, Beams 2-7 were loaded at an increased range of 40 kN - 100 kN. The same cyclic loading was applied to each beam, regardless of strengthening level, as this represents the most realistic situation where a RC girder would be repaired with CFRP and the same loading cycle would be present before and after the repair. Two slower cycles, at a frequency of 0.05 Hz, were applied to the beam at the first two cycles and every 50,000 cycles afterward. These slow cycles allowed for a more refined data set to be collected, approximately 56 scans per slow cycle, and allowed for the digital microscope to be switched to both sides of the beam to view the most exterior No. 19 bars. For Beam 1, with no concrete void, the number of slow cycles was set to a single cycle since pictures could not be taken with the digital microscope. Table 3.1 gives a summary of the test beam variations.

Table 3.1 Summary of experimental beam variations

	Concrete Void	Rebar Strain Gages	CFRP
Beam 1	No	One on each No. 19 at mid-span, 3 total	None
Beam 2	Yes	One on each No. 19 at mid-span and 400 mm off center, 6 total	None
Beam 3	Yes	One on each No. 19 at mid-span and 400 mm off center, 6 total	None
Beam 4	Yes	One on each No. 19 at mid-span, 3 total	Tyfo SCH-41 Sheet
Beam 5	Yes	One on each No. 19 at mid-span, 3 total	Tyfo SCH-41 Sheet
Beam 6	Yes	One on each No. 19 at mid-span, 3 total	Tyfo UC Strip
Beam 7	Yes	One on each No. 19 at mid-span, 3 total	Tyfo UC Strip

3.2.2 Specimen Design

All test beams were designed with the same dimensions and internal steel reinforcement using ACI-318: Building Code Requirements for Structural Concrete. Length of the specimens was controlled by the size of the testing frame. From there the depth was chosen to ensure the beam didn't fall under deep beam conditions, and a width picked to produce a rectangular cross-section, which is typical for RC beams and agreed well with previous research. Adequate concrete cover was also taken into account when dimensioning the beam cross-section. The steel reinforcement amount was chosen to produce an under-reinforced beam, which would fail in flexure. While compression reinforcement wasn't needed for strengthening purposes, fabrication of the reinforcing cages was easier with them. Additionally, since the beams were to be fabricated in an inverted position so the FRP could be applied to the tensile soffit of the beam, the compression bars were needed to provide a place for the rebar chairs to elevate the cage off the bottom surface of the forms. The shear stirrups were needed in order to resist diagonal-shear cracking, which would have been the controlling failure mode at the given loadings.

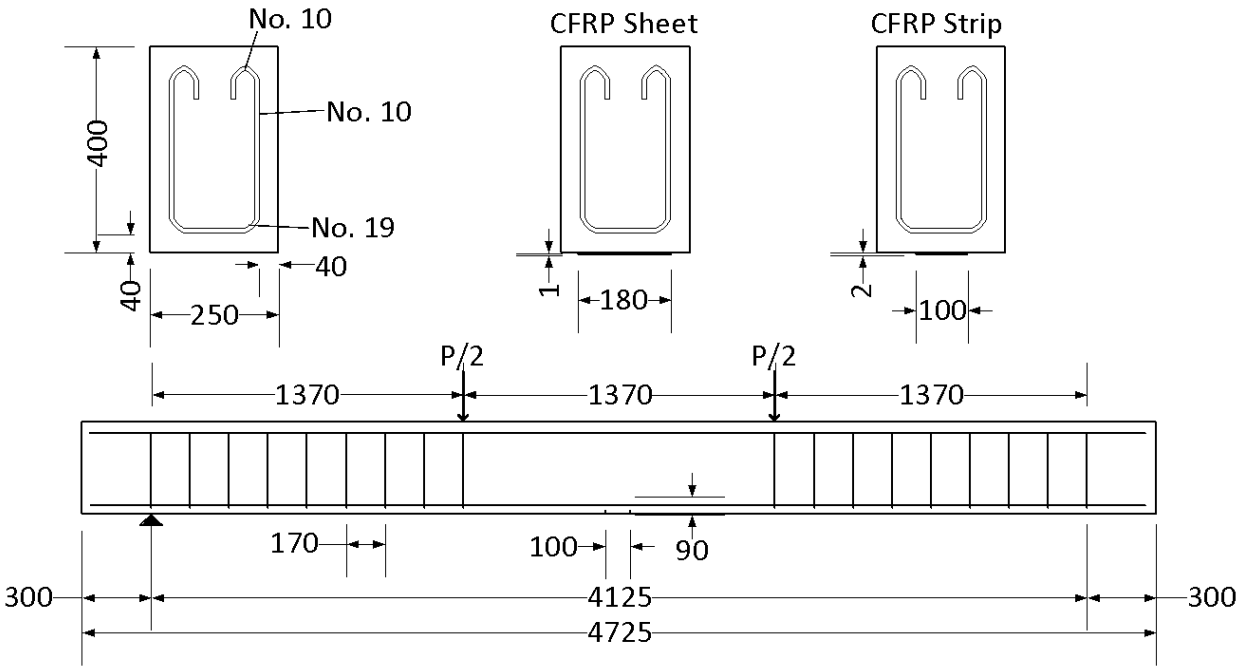

Figure 3.10 Experimental test specimen details

The notch cut into the tensile reinforcement was sized using Equation 10 to represent a corrosion pit, which would have formed in a highly corrosive environment at a very localized point, such as a flexural crack in the concrete, over 20 years. This gave a notch depth of approximately 2 mm. This value was checked with Equation 5 and Equation 4 to ensure this notch would be able to produce a stress intensity factor range higher than the threshold value, allowing fatigue crack growth.

In order to investigate the difference in designing an FRP repair for strength versus fatigue, the beams in groups 3 and 4 were both repaired to the same nominal moment carrying capacity using Equation 10-13 from ACI 440.2 with two different CFRP types. The beams in group 3 (4 and 5) were strengthened using a CFRP sheet while the beams in group 4 (6 and 7) were strengthened using a CFRP prefabricated strip. Since it was easier to vary the width of the CFRP sheet, the moment capacity for a beam strengthened with the CFRP strip was determined, then the width of the CFRP sheet, which would be able to provide the same strength, was determined. The factored nominal moment capacity for beams 1, 2, and 3 was found to be 115.9 kN-m, for beams 4 and 5 the capacity was found to be 150.26 kN-m, and for beams 6 and 7, 150.19 kN-m was calculated. Whereas the moment capacity of the unstrengthened beams was governed by yielding of the steel rebars, the moment capacity of both types of strengthened beams was governed by the debonding of the CFRP. In the strengthened beams, the yield strain of the steel rebars is reached first followed by the predicted debonding strain of the CFRP while the concrete strain remains below the ultimate strain until after the CFRP debonds.

The applied load range between 40 kN and 100 kN gave a predicted stress range in the tensile steel reinforcement of 150 MPa for the unstrengthened beams, 130 MPa for the Tyfo SCH-41 strengthened beams, and 120 MPa for the Tyfo UC strengthened beams. These values were obtained using equation 10-14 from ACI 440.2 and general section analysis calculations.

Equation 13. Stress in steel reinforcement under service loads (ACI 440.2)

$$\sigma_{s,s} = \frac{\left[M_s + \varepsilon_{bi} A_f E_f \left(d_f - \frac{kd}{3}\right)\right](d - kd)E_s}{A_s E_s \left(d - \frac{kd}{3}\right)(d - kd) + A_f E_f \left(d_f - \frac{kd}{3}\right)(d_f - kd)}$$

3.2.3 Specimen Fabrication

The test beam specimens were fabricated in the structural engineering lab at the Colorado State University Engineering Research Center directly adjacent to the testing frame. Formwork was constructed out of 19-mm-thick plywood and 2x4 lumber, shown in Figure 3.11. The formwork was assembled in such a way so that the walls could be removed after the concrete had cured so application of the CFRP could occur and the beams could be picked up and individually loaded into the testing frame.

Figure 3.11 Braced plywood and lumber form-work

In addition to the walls and bottom of the formwork, foam tubes were used to form a 90-mm-deep and 100-mm-wide cylindrical void into the concrete to expose the No. 19 tensile rebars at mid-span of beams 2-6, which allowed access for a digital microscope to track the crack growth rate, as shown in Figure 3.12. Again the beams were fabricated in an inverted position to allow access to the tensile soffit of the beam for FRP application; therefore, the voids were cast in the relative top of the beams. The void in the concrete offset relative to the notch at mid-span to allow the nominal strain in the rebar in the void to be measured via a strain gage. In order to keep the strain gage away from any stress concentration cause by the notch while also keeping the void to a minimal size the void was offset.

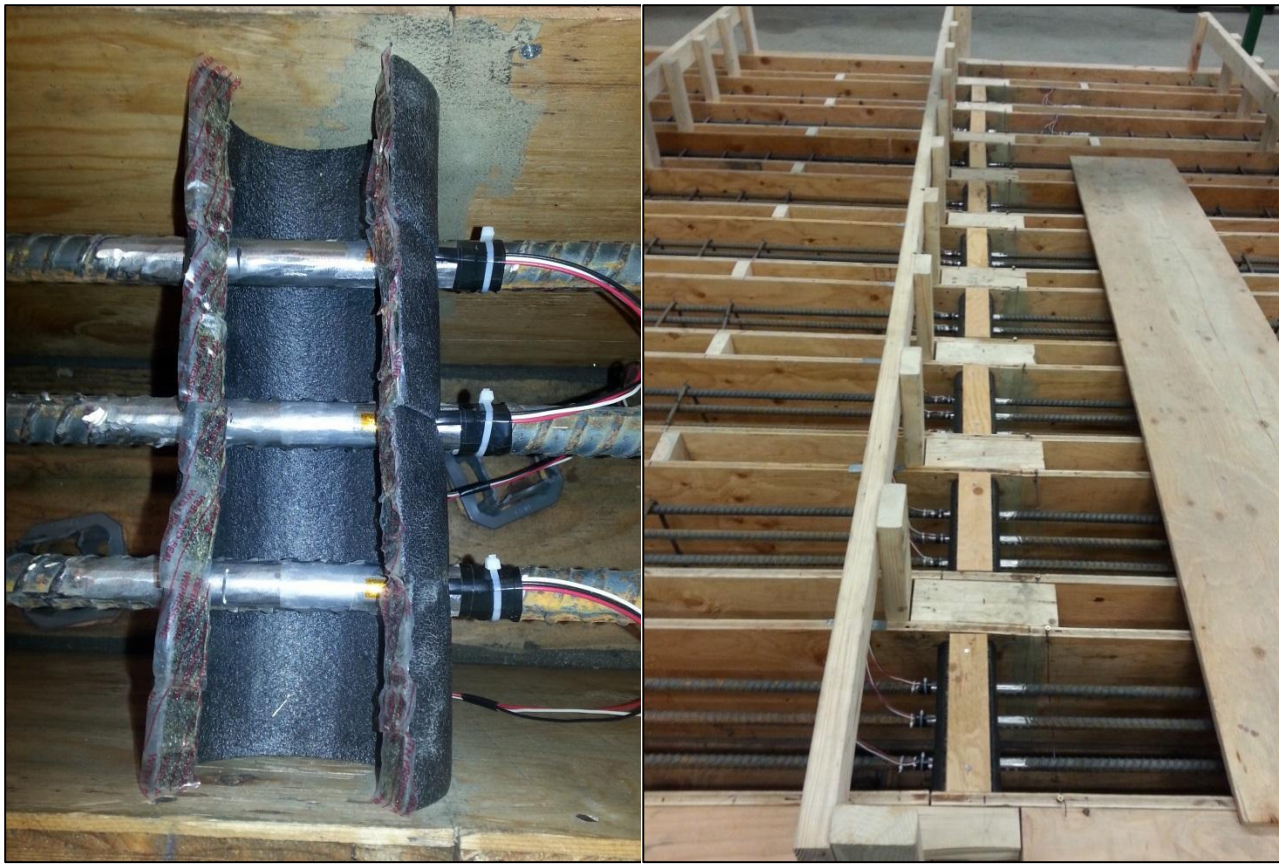

a) b)

Figure 3.12 a) Foam tube used to form void at mid-span, shown with notches cut in outermost rebars, b) Foam void forms with lumbar caps in beams 2-10.

The steel rebar cages were tied up and lowered into the forms with the No. 19 rebars on the relative top. The cages rested on plastic rebar chairs in order to achieve the concrete cover needed as shown in Figure 3.13 b). Once the cages were in the forms the ribs on the No. 19 rebars were removed for a length of 150 mm at mid-span and in beams 2 and 3 at an additional location 230 mm away. The purpose for these additional smoothed portions is explained later in the Instrumentation section. The ribs were removed and the surface polished not only to give the strain gages a smooth surface to attach to but also so propagation of a fatigue crack from the cut notch would be more easily visible. The notches were cut into the outermost No. 19 rebars after polishing using a Dremel tool with a silicon carbide cutoff wheel with a marking of 2 mm to ensure all notches were cut to approximately the same depth. A rounded notch tip was left by the cutting wheel; therefore, a utility knife blade was used to sharpen the notch tip to preserve the higher stress intensity.

a)

b)

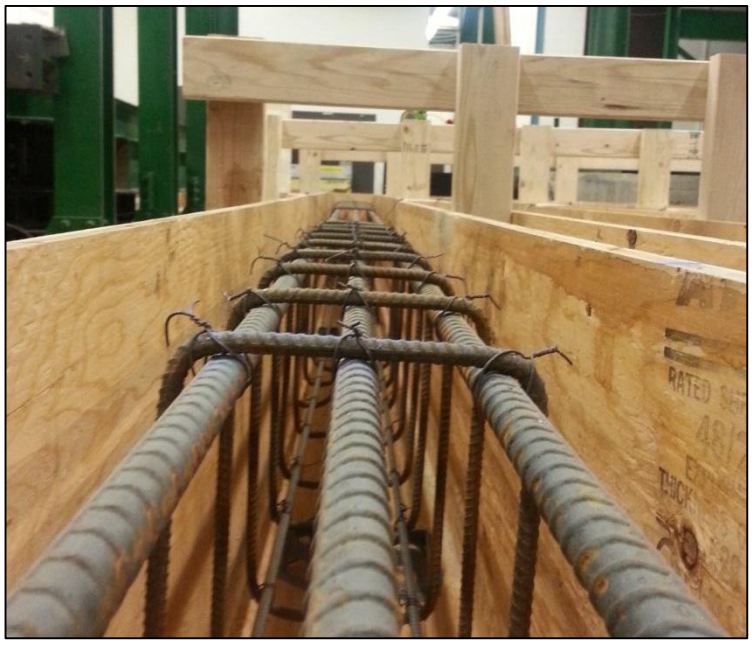

c)

d)

Figure 3.13 a) Rebar cages, b) 40-mm plastic rebar chairs, c) position of rebar cage in form, d) depth of tensile reinforcement once supported on 40-mm rebar chairs

The concrete was supplied by a local concrete batch plant and placement of the concrete for all beams was performed in the same day as shown in Figure 3.14. A concrete vibrator, shown in Figure 3.14, was used to ensure minimal voiding between the rebar cages and form walls as well as around and in the rebar chairs. The concrete was allowed to cure for 28 days before the formwork was removed and testing began.

Figure 3.14 Concrete placement

Application of the CFRP didn't occur until the concrete reached the 28-day compressive strength. Four beams were externally strengthened with commercially available CFRPs produced by Fyfe Co. Prior to application of any CFRP, a diamond cup grinding wheel was used to remove the concrete laitance layer (about 5 mm) from the soffit of each beam to expose the aggregate and promote a stronger bond between the concrete and CFRP as shown in Figure 3.15. Beams 4 and 5 were strengthened with a 190-mm-wide Tyfo SCH-41 unidirectional carbon fabric sheet and Tyfo S Epoxy. The fabric sheet was saturated with the epoxy and applied to the prepared beams via a hand lay-up process shown in Figure 3.16. Beams 6 and 7 were strengthened with a single Tyfo UC strip, which is a high modulus, high tensile strength, pultrusion fabricated carbon-epoxy laminate. The Tyfo UC strips were adhered to the concrete substrate with Tyfo TC Epoxy as shown in Figure 3.17.

Figure 3.15 Concrete surface, top) removed laitance layer exposing aggregate, bottom) concrete surface left by finishing of wet concrete

Figure 3.16 Hand-layup process of Tyfo SCH-41 CFRP sheets and beams 4 and 5

Figure 3.17 Tyfo UC CFRP strip

3.2.4 Material Properties

The concrete was allowed to cure for 28 days. Cylinder compression tests were performed at 7, 14, and 28 days. In addition, a test was performed at the halfway point through testing. At each testing day, three cylinders were tested to determine an average value. The results were then used to produce a compressive strength curve so the concrete compressive strength for each beam could be determined the day the specimen was tested. In Table 3.2, the values for the compressive strength are the average of each beam in the group. Properties for the CFRP and steel reinforcement are also given. Detailed mill certificates for the steel rebars are provided in Appendix A.

Table 3.2 Experimental beam material properties

Material Properties	Unstrengthened Beams 1,2, and 3	Tyfo® SCH-41 Sheet Beams 4 and 5	Tyfo® UC Strip Beams 6 and 7
Concrete compressive strength (MPa)	32.82	33.23	33.35
Rebar Tensile Yield Strength No. 10/No.19 (MPa)*	491/481	491/481	491/481
CFRP Tensile Strength (MPa)*	N/A	986	2790
CFRP Tensile Modulus (GPa)*	N/A	82	140
CFRP Elongation at Break (%)*	N/A	1.0	1.8
CFRP Width (mm)	N/A	190	100
CFRP Thickness (mm)	N/A	1	2
Epoxy Tensile Strength (MPa)*	N/A	72.4	22.7
Epoxy Tensile Modulus (GPa)*	N/A	3.18	1.2

* Properties provided by manufacturer

3.2.5 Test Setup and Instrumentation

All beams were loaded at clear-span third points, 1,370 mm from each support, through a spreader-bar by a single 160 kN capacity MTS servo-hydraulic actuator as shown in Figure 3.18 a). The actuator was controlled using an MTS Flex test GT whose control software was configured to collect the applied load, actuator extension, and cycle count data at each load cycle peak and valley. Linear pots mounted to the beam at mid-span and at each loading point provided direct measurement of beam displacements. Foil-backed 350Ω strain gages were attached to each No. 19 rebar 65 mm from the notch cut at mid-span. Beams 2 and 3 had additional strain gages attached to the No. 19 rebars 400 mm off from mid-span for strain comparison purposes within the constant moment region. In addition, a single strain gage was attached to the concrete surface on top of each beam at mid-span and two strain gages were applied to the CFRP within the constant moment region, one directly over the void and the other 230 mm away. All instrumentation was wired to Campbell Scientific CR1000 data loggers for data collection.

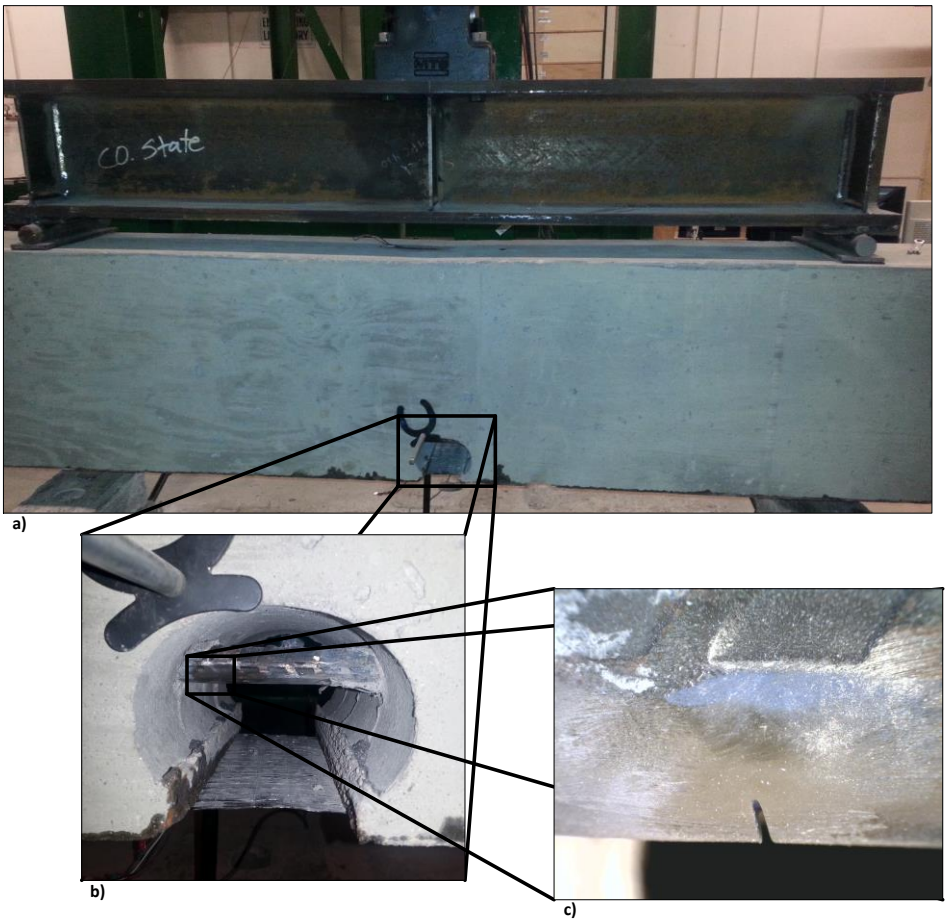

Figure 3.18 a) Constant moment region of beam showing loading apparatus at top and void in concrete exposing tensile rebars, b) void showing CFRP sheet (bottom center) and digital microscope mount (top left), and c) notch and polished surface of rebars at mid-span

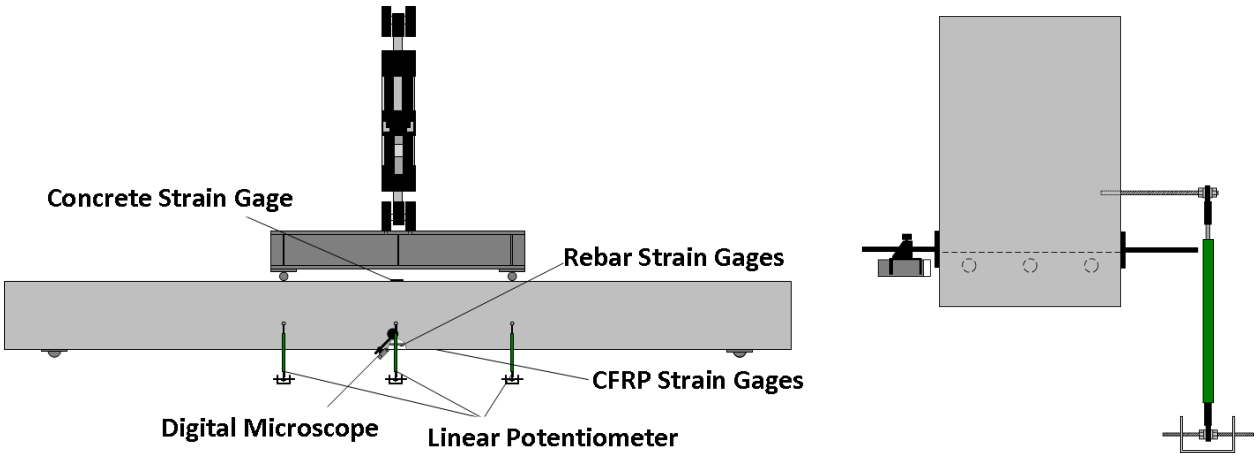

Figure 3.19 Loading and instrumentation set-up a) beam profile view, b) beam end view

Crack length measurements were made using a Dino Lite digital microscope. The microscope was attached to the side of the beam allowing for a profile image at approximately 20 times magnification to be taken of the rebars closest to the sides of the beam, as shown in Figure 3.19. Based on the magnification, dimensions of the crack could be measured from the image using companion software. Fatigue cracking would only be able to be measured along the side facing circumference of the rebar, which would still give accurate results since the crack growth rate and not the absolute crack length was more of a concern.

4. RESULTS AND ANALYSIS

4.1 Concrete Void Comparison

The significance of the rebar access void in the concrete with respect to the structural performance of the beam was first considered. Figure 4.1 shows the secant stiffness of each beam throughout the fatigue test. The secant stiffness is defined as the slope of the load-deflection curve during cycling. Comparing Beam 1 to Beams 2 and 3 (those with no CFRP, but with a void in the concrete) indicates the addition of the void decreases the member stiffness by about 4.5%. The plot indicates that the stiffness of Beam 1 is more similar to Beams 4 and 5 (those strengthened with the SCH-41 CFRP) than it is to Beams 2 and 3. This result is contrary to that of the small scale testing, which showed negligible difference in stiffness between the beam with no void and the ones with a void.

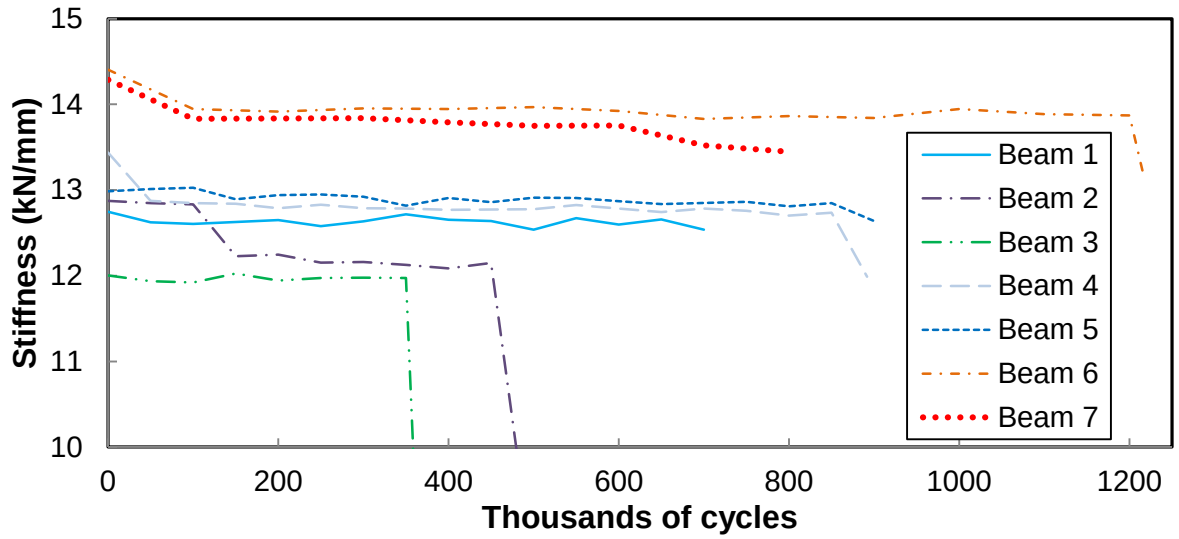

Figure 4.1 Secant stiffness vs. number of cycles

The effect the void had on the measured rebar strains was also investigated in Beams 2 and 3. Figure 4.2 and Figure 4.3 show the comparison between the strain ranges in the three tensile rebars both inside the void and embedded in the concrete at a location 100 mm away for Beams 2 and 3, respectively. The lower measured strain values in Beam 2 are attributed to the higher stiffness of Beam 2 at the 50,000 cycle mark when the strain values in Figure 4.2 and Figure 4.3 were taken. These strain ranges were only assessed at this point because shortly after the 50,000 cycle mark the rebar strain gages embedded in concrete started to fail due to flexural cracking of the concrete, causing the lead-wires to pull away from the gages. These plots show for both beams the stress ranges in the void were noticeably higher than in the concrete despite both locations being within the constant moment region. This result differed from that found for the small beam test, which showed similar load-strain rates within the elastic region along the beam's length. However, the post-yield strain measured in the rebar embedded in concrete was lower than the rebar in the void, which agrees with the trend in the large scale beams. While these results from the large scale beam tests indicate that the void did have an impact on the structural performance of the beams, the degree of this impact was minor, especially for the purpose of the study, which focused on the comparison of the CFRP repairs on the beams, all of which had voids in the concrete. Additionally, strain measurements were made within the void near the location of the notch, where rebar crack growth occurred, allowing the nominal stress at the location of the crack to be determined.

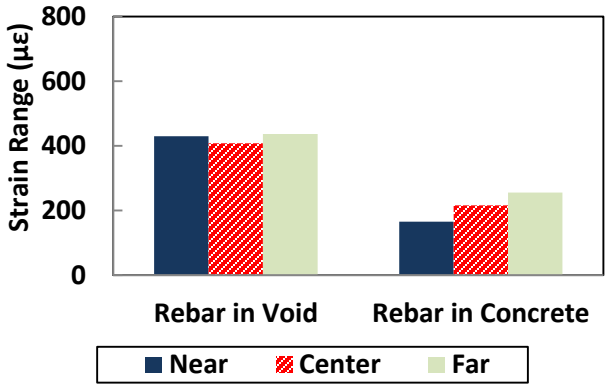

Figure 4.2 Beam 2 rebar strain ranges

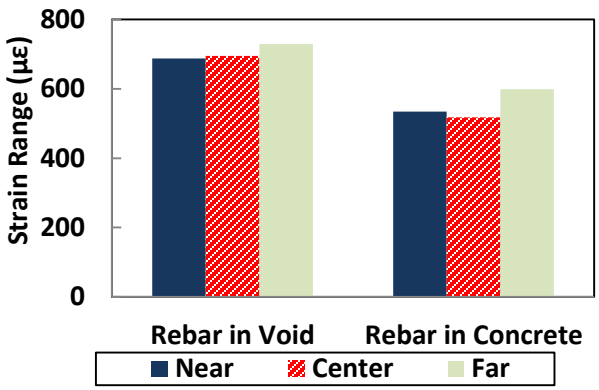

Figure 4.3 Beam 3 rebar strain ranges

While the exact cause for the differing results between the small scale and full scale beams is unknown, a portion of the discrepancy might have been caused by the location of the strain gages in the voids. In the small beams, the strain gages were located centrally in the void while in the full scale beams, the gages were near the edge of the void, which might have caused a stress concentration resulting in the higher strain readings. However, this only explains the difference in strain and not the stiffnesses.

4.2 Observed Behavior

All beams, with the exception of Beam 1, failed due to fatigue induced fracture of one or more of the notched tensile No. 19 bars, Figure 4.4. It is believed Beam 1 did not show signs of fatigue due to the smaller stress range that was produced from the loading and the fact that the notches in the rebar were not sharpened with the utility blade prior to concrete placement, resulting in a notch tip that did not produce a sufficiently high stress intensity factor range to promote crack extension. Beams 2 and 3 both experienced fatigue crack growth in both notched rebars, while in Beams 4-7 fatigue crack propagation only occurred in one of the notched bars despite continuing the testing for a minimum of 50,000 cycles after the fracture of the first rebar. In Beams 2 and 3, presence of a visible crack in the other notched rebar occurred prior to fatigue induced fracture of the rebar, which first showed crack growth. Additionally, the number of cycles between fracture in both rebars in Beams 2 and 3 was less than 50,000 cycles. Immediately following fracture of the second notched rebar, the third, middle rebar yielded, and development of large flexural cracks extending from the concrete void ensued, as shown in Figure 4.5. The propagation of the fatigue crack that occurred in Beam 6 is shown in Figure 4.6.

Figure 4.4 Fatigue induced fracture of tensile No. 19 rebar

Figure 4.5 Large flexural cracking occurring immediately after fracture of second rebar in beams 2 and 3

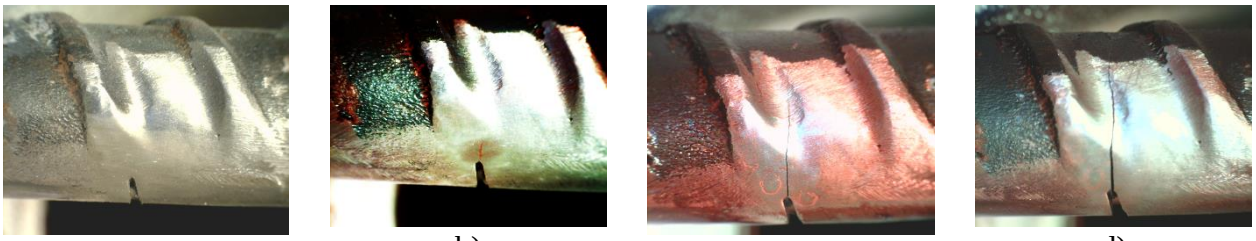

a) b) c) d)

Figure 4.6 Progression of fatigue crack growth in beam 6. a) 600,000 cycles, no cracking, b) 1,050,000 cycles, 1.702 mm crack, c) 1,200,000 cycles, 8.392 mm crack, d) 1,214,700 cycles, fracture

The addition of both CFRP repair systems was observed to reduce the strain in the tensile reinforcement. The average rebar strain range in Beams 2 and 3 was 564.55 με, however an observed decrease of 16.2% was present in Beams 4 and 5 strengthened with the Tyfo SCH-41 sheet, and a decrease of 19.6% was present in Beams 6 and 7 strengthened with the Tyfo UC strip, as shown in Figure 4.7. The addition of Tyfo SCH-41 increased the beam stiffness by 6.85% and the Tyfo UC strips increased the stiffness by 15.31% over the unrepaired beams. The difference in the increased stiffness and the decreased stress dange in the repaired beams show that increasing the stiffness due to the application of CFRP doesn't necessarily ensure a proportional decrease in the stress range the steel reinforcement experiences.

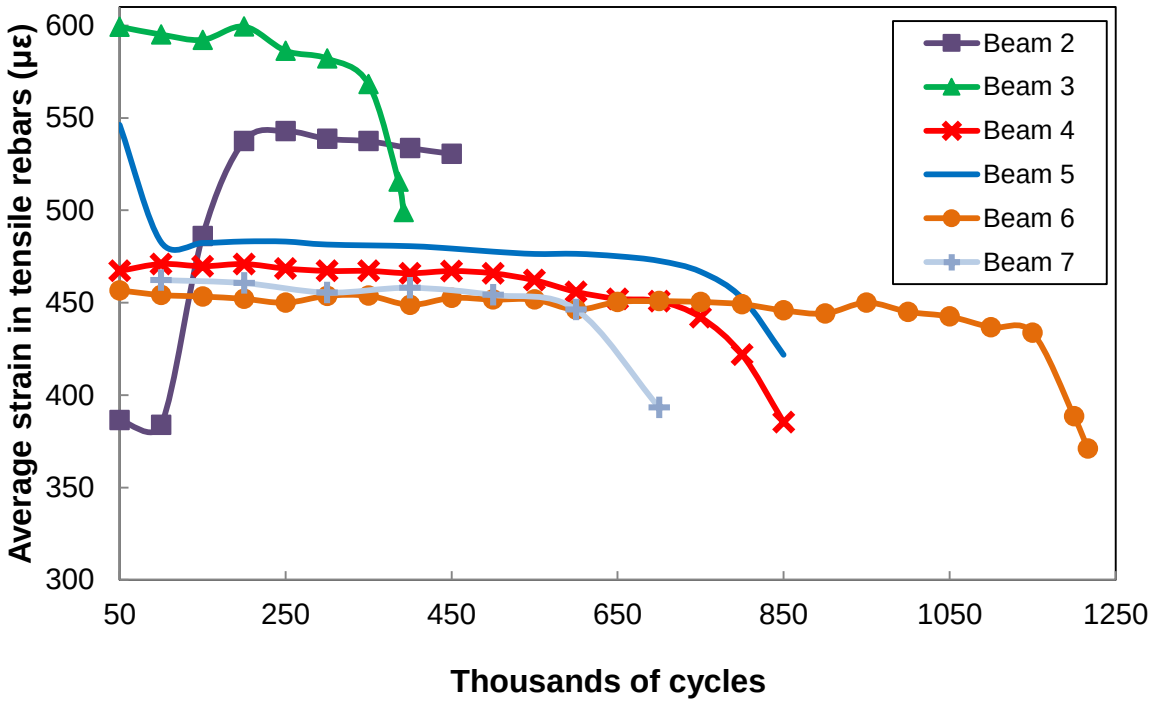

Figure 4.7 Average tensile rebar strain range during fatigue test

The presence of different strain/stress ranges in the two CFRP systems, despite being designed for the same flexural capacity, indicates there might be is a slight difference in applying a CFRP repair for strengthening and fatigue. This finding further emphasizes the need for design provisions for fatigue and not just using strength designs to provide increased fatigue performance.

Just prior to any cracking in the rebar becoming observable with the digital microscope, a drop in the measured strain would occur. This drop was linear at first, but after the crack length exceeded 3 mm the drop became exponential with continued cycling. Additionally, as the strain in the fatiguing bar would drop the strain in the other two bars would increase, signifying a redistribution of stresses.

It was interesting to observe that although the notches were sharpened and theoretical calculations showed the stress intensity factor range was higher than the threshold value of 3.3 MPa√m, crack propagation was not observed for a significant number of cycles in each beam, showing that despite the attempt to achieve crack growth from the first cycle crack initiation still needed to take place.

Finally, despite Kim and Heffernan (2008) reporting many studies experiencing issues with debonding of the FRP along the beam's length, especially with thicker and high modulus FRPs, no debonding of any type was observed in this study. This was to be expected, as the measured strains in the CFRP never exceeded 0.0017e, which was below the calculated value at which debonding would occur of 0.0045e. It is believed end-peel debonding was prevented by extending the CFRP sheets/strips to beyond the supports, creating a mechanical clamping action when the beam was loaded. While cracking was observed in the thicker Tyfo TC epoxy used on Beams 6 and 7 at locations of flexural cracking of the concrete, debonding was limited to just over the crack and did not extend away from the crack along the beam's length.

4.3 Fatigue Life and Crack Growth Rate

Figure 4.8 and Figure 4.9 show the crack length vs. number of cycles for each beam over the entire test and from the point where the crack first becomes visible, respectively. A general trend of increased fatigue life and slowed crack growth rate with the addition of CFRP can be seen. It is inconclusive, however, as to whether there is improved performance with either CFRP sheets or strips in regard to these parameters. Both the fatigue life and crack growth rate for the SCH-41 sheet strengthened beams (4 and 5) are very consistent; however, the differences in both parameters for the UC strip strengthened beams (6 and 7) are significant. Beam 6 shows improved performance over the SCH-41 system with a longer fatigue life and slowed crack growth rate. Conversely, Beam 7 shows worse performance, with a shorter fatigue life and a quicker crack growth rate. Therefore, the experimental results of this study are not enough to determine if there is a difference in designing CFRP repairs for strength and repairs for fatigue, despite the theoretical calculations and a slight difference in the experienced stress range in the rebar showing otherwise.

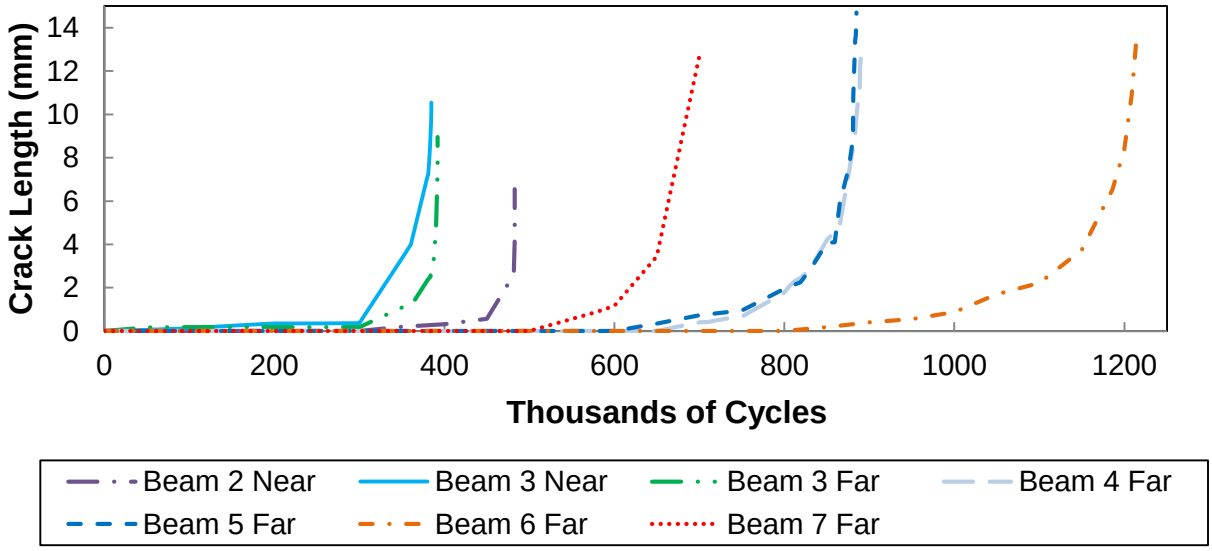

Figure 4.8 Crack length vs. number of cycles

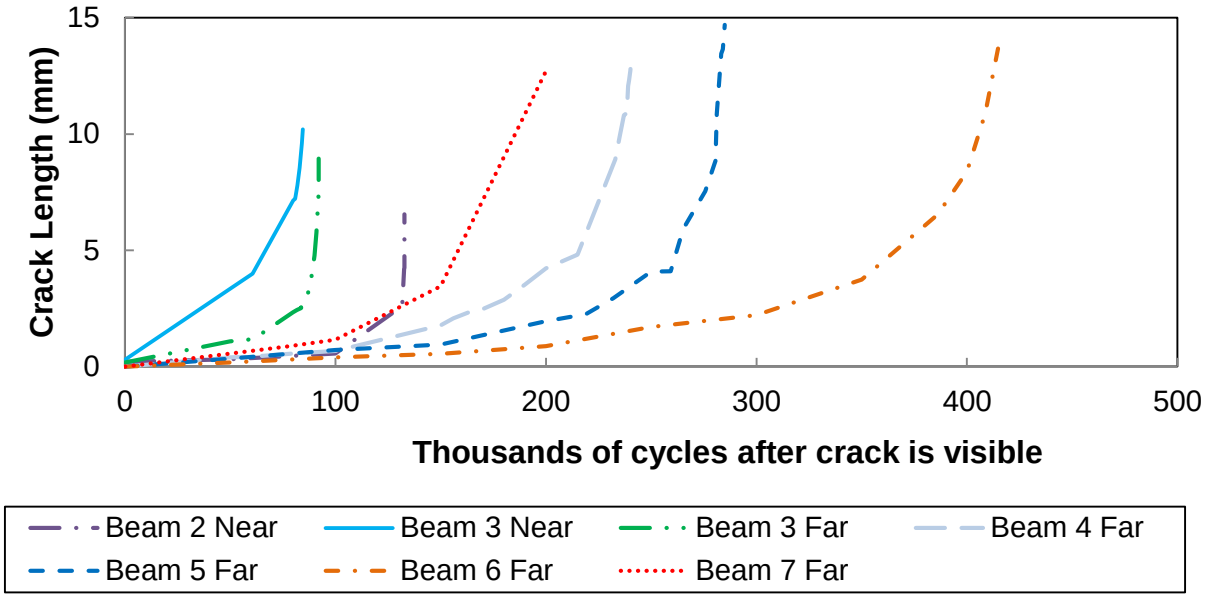

Figure 4.9 Crack length vs. number of cycles after the crack is visible

4.4 Fatigue Parameter Analysis

The Paris Law constants, *C* and *m*, were determined from a log-log plot of the crack growth rate, da/dN, versus the stress intensity factor range, ΔK, for each beam as shown in Figure 4.10. The values for *C* and *m* are the y-intercept and slope of the power trend line shown on the plot, respectively. The R^2 value for this trend line was 0.803. The value for *C* was determined to be 1.435E-10, below the conservative value for this type of steel of 3.6E-10 proposed by Barsom and Rolfe (1999), while the value for *m* was found to be 2.2375, which is slightly below the well-accepted average value of 3. It should be noted that these values were obtained after the outliers of the data set were removed. Large ΔK and da/dN values were removed because these points correspond with large crack lengths, which were assumed to be well outside the stable crack growth region, which is described by the Paris Law. Therefore, the removal of these values was theoretically needed as they cannot be described by the Paris Law. It is believed the determined constants varied from the well-established values due to the high tolerance needed for measuring the crack length, which was often difficult to accurately determine due to the extremely small size of the crack.

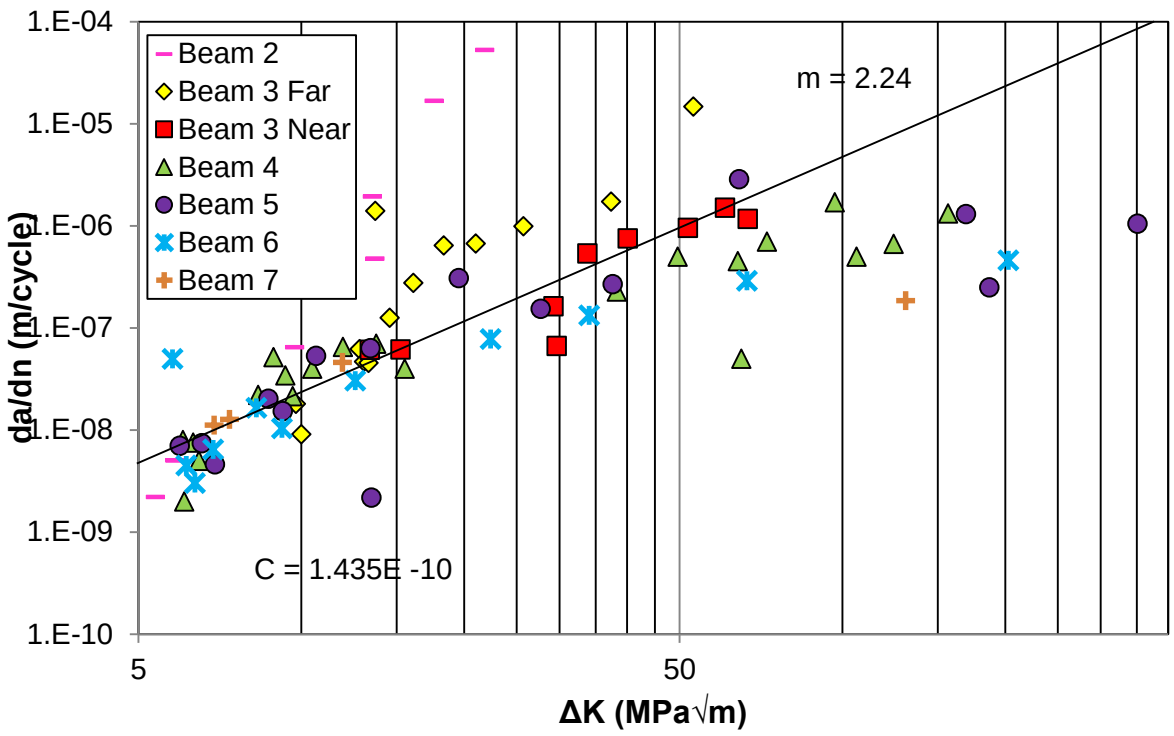

Figure 4.10 Crack propagation rate vs. stress intensity factor range

The fracture toughness, K_{IC}, was found by solving Equation 3, where the max stress and critical crack length were obtained experimentally from each specimen and the value of *F* for the crack correction factor was determined for the critical crack length. The average K_{IC} value from all tests was found to be 113.35 MPa√m. This value was validated by a Charpy V-notch test, which consisted of testing five specimens milled from the core of a leftover piece of the No. 19 tensile bars. The average fracture determined from the CVN test was 104.4 MPa√m.

With these material constants determined from the data, a comparison between the actual and predicted fatigue lives could be performed in order to evaluate the accuracy and applicability of these values. Table 4.1 compares the actual fatigue life from the experimental study to the predicted fatigue life using Equation 9 with the published and calculated values for *C* and *m*.

The results show the published values for the material constants by Barsom and Rolfe greatly underestimate the fatigue life, with an average percent of actual of 12.6%. The values determined from this study overestimated the fatigue life by a fair amount, with an average percent of actual of 163%. A portion of the overestimation is believed to be because the number of cycles from the experimental tests only account for cycles from first observation to fracture of the rebar, whereas the predicted values, being calculated from the Paris Law equation, account for every cycle within the stable crack growth region whether or not it was visible from a profile view. It is believed the predicted values from the determined constant values and actual fatigue lives would be much closer if the number of cycles to fracture from the very first bit of crack growth could be determined. This is because the initial very first cycles actually take the largest number of cycles to grow because of the small stress intensity factor value.

Table 4.1 Number of cycles from first crack detection to fracture

	Experimental Fatigue Life	Predicted Fatigue life using Theoretical C and m values	% of Actual	Predicted Fatigue Life using Determined C and m values	% of Actual
Beam 2	132,794	30,530	23	343,811	259
Beam 3 Near	84,800	13,113	15	189,579	224
Beam 3 Far	92,100	12,093	13	180,717	196
Beam 4	240,500	24,558	10	306,403	127
Beam 5	285,000	24,852	9	308,826	108
Beam 6	414,700	24,206	6	303,461	73
Beam 7	198,400	23,625	12	298,185	150

5. RECOMMENDATIONS, FUTURE WORK, AND CONCLUSIONS

5.1 Recommendations

A means of designing an FRP repair for flexural RC members that addresses the fatigue performance of the repaired member and not solely the static strength is needed. The use of well-established fracture mechanics equations along with the preexisting design guidelines in ACI 440.2 allows for a design method that explicitly considers the way FRP repaired members loaded in fatigue are most likely to fail, i.e., through fatigue failure of the reinforcing steel. The following flowchart, Figure 5.1, is proposed to allow the design engineer to specify the desired extension in the fatigue service life, and using fatigue parameters such as those obtained from this study, average daily truck traffic and properties of the bridge girders determine the amount and mechanical properties of FRP needed in order to achieve the desired life extension. The flowchart is broken into four general segments: a) *Known Parameters*, b) *FRP Repair Design*, c) *FRP Repair Properties*, and d) *Fatigue Evaluation*. Use of the proposed flowchart first requires establishing values for variables in the *Known Parameters* segment, which are grouped into three categories: *Girder Properties*, *Bridge Characteristics*, and *Fatigue Properties*. Next the *Fatigue Evaluation* side of the flowchart must be solved to determine the stress range in the rebar the FRP repair must reach in order to get the desired fatigue life extension referred to as $\Delta\sigma_{needed}$. In order to find this value, the number of loading cycles within the extended life, N_{ext}, and the critical crack length must be determined. N_{ext} is simply found by multiplying the average daily truck traffic, *ADTT*, by 365 days in a year and by the number of years the repair is to extend the fatigue life. The a_c term is calculated using Equation 6. Since this equation requires σ_{max} in the tensile rebar after the FRP repair, which is still unknown, an initial estimated value, σ_{max}*, is needed. Most repair schemes have resulted in σ_{max} values after FRP repair being 75%-90% of the unrepaired maximum; however, any reasonable value is adequate since at a later point σ_{max}*is adjusted and the design can be performed again to achieve convergence. Since *F* is dependent on the crack length, but the crack length throughout the fatigue life isn't known, the average value of *F* for the initial crack length and the critical crack length was taken to be *F*. Once N_{ext} and a_c are found, a reworked form of the Paris Law equation can be used to find $\Delta\sigma_{needed}$.

Equation 14. Stress range in steel rebar FRP repair must achieve. Derived from the Paris Law equation

$$\Delta\sigma_{needed} = \frac{\sqrt[m]{\frac{2\left(a_c^{\frac{2-m}{2}} - a_i^{\frac{2-m}{2}}\right)}{N(2-m)C}}}{F\sqrt{\pi}}$$

Now the process shifts to the *FRP Repair Design* side of the flowchart in order to plan a design that will provide a stress range, $\Delta\sigma_{provided,}$ in the tensile rebars at or below the $\Delta\sigma_{needed}$ level. Preliminary values for the area of FRP, A_f, effective depth of the FRP, d_f, and the modular ratio of FRP to concrete, n_f, are calculated. These values along with the dead load moment, M_D, and dead plus live load moment, M_{D+L}, are then used in section analysis calculations to determine ratio of depth of the neutral axis to steel reinforcement depth measured from the extreme compression fiber, k. Once this value is known for both design loads, the maximum, σ_{max}, and minimum stress, σ_{min}, in the steel rebars can be calculated using Equation 13. At this point, the σ_{max} value that has been determined should be checked with the σ_{max}* value first used to find $\Delta\sigma_{needed}$. If the values are different, the *Fatigue Evaluation* side of the flowchart should be revaluated, plugging in σ_{max} for the initial σ_{max}* value until convergence is achieved between σ_{max}* and σ_{max}. Next $\Delta\sigma_{provided}$ is determined from σ_{max}, and σ_{min},and check against $\Delta\sigma_{needed}$. If $\Delta\sigma_{provided}$ is lower than $\Delta\sigma_{needed}$ the design is adequate but overly conservative, therefore the area and/or modulus of the reinforcement should be lower; if the converse is true, and the provided stress range is too low, then the area and/or modulus should be increased until the stress ranges agree. Once agreement is reached, the design should be checked with the remainder of the ACI 440.2 provisions for strain limits in between each component.

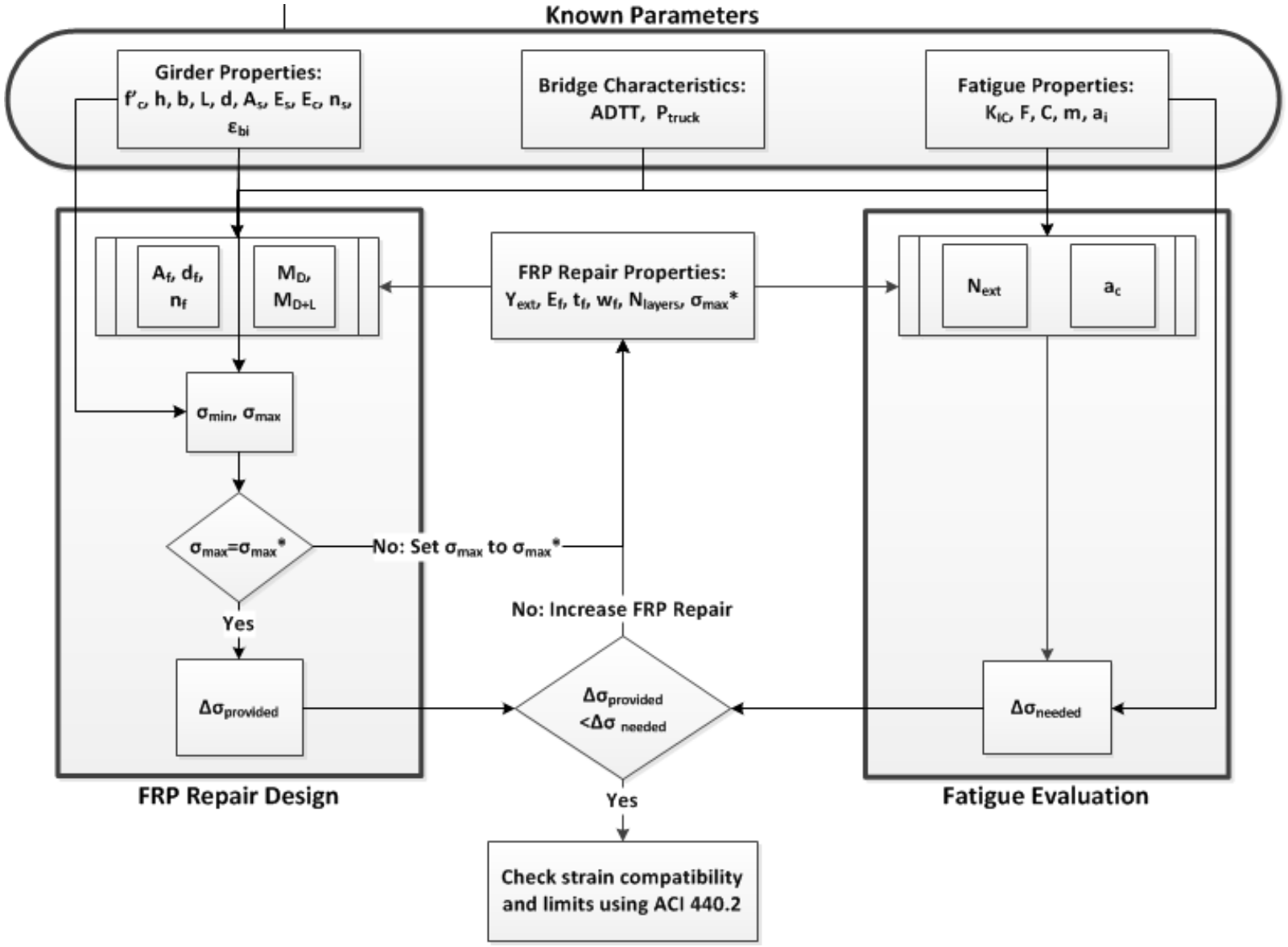

Figure 5.1 Proposed fatigue design flowchart for FRP repair of RC flexural members

Table 5.1 Variable definitions and units

ADTT	=	average daily truck traffic (trucks/day)	M_D	=	Dead load moment (kN-m)
A_f	=	area of FRP external reinforcement (m^2)	M_{D+L}	=	Dead plus live laod moment (kN-m)
A_s	=	area of tensile steel reinforcement (m^2)	m	=	Paris Law material constant
a_c	=	critical crack length (m)	N_{ext}	=	Number of cycles repair extends fatigue life (cycles)
a_i	=	initial flaw length (m)	n	=	Number of plies of FRP reinforcement
b	=	width of member (m)	n_f	=	Modular ratio of elasticity between FRP and concrete
C	=	Paris Law material constant	n_s	=	Modular ratio of elasticity between steel and concrete
d	=	distance from extreme compression fiber to centroid of tension reinforcement (m)	P_{truck}	=	Design truck load (kN)
d_f	=	effective depth of FRP flexural reinforcement(m)	t_f	=	Nomial thickness of one ply of FRP reinforcement (m)
E_c	=	modulus of elasticity of concrete (MPa)	w_f	=	Width of FRP reinforcing ply (m)
E_f	=	Tensile modulus of elasticity of FRP (MPa)	Y_{ext}	=	Years FRP repair is to extend fatigue life (years)
E_s	=	Modulus of elasticity of steel (MPa)	$\Delta\sigma_{needed}$	=	Stress range in steel reinforcement needed to ensure fatigue cracks don't reach critical value within extended life (MPa)
F	=	Crack shape factor	$\Delta\sigma_{provided}$	=	Stress range in steel reinforcement after FRP repair (MPa)
f'_c	=	Specified compressive strength of concrete (MPa)	ε_{bi}	=	Strain level in concrete substrate at time of FRP installation (m/m)
h	=	Overall height of member (m)	σ_{max}	=	Maximum stress in steel reinforcement after FRP repair produced by M_{D+L} (MPa)
k	=	Ratio of depth of neutral axis to reinforcement depth measured from extreme compression fiber	σ_{max}*	=	Initial predicted value of maximum stress in steel reinforcement after FRP repair (MPa)
K_{IC}	=	Fracture toughness or critical stress intensity factor (MPa$\sqrt{m}$)	σ_{min}	=	Minimum stress in steel reinforcement after FRP repair produced by M_D(MPa)
L	=	Flexural member length (m)			

An assessment of the proposed flowchart was performed using the beams from the experimental study along with the determined fatigue parameters. Setting N_{ext} to the number of cycles determined from the experimental study, a_i to the initial notch depth cut into the rebars, σ_{max}*to the values measured during fatigue testing and using the determined values for *C* and *m*, $\Delta\sigma_{needed}$ was determined. The modulus and amounts of each type of CFRP repair were used along with the material and geometric properties of the beams to determine $\Delta\sigma_{provided}$ and the corresponding number of cycles the repair provided using Equation 9. Table 5.2 shows the obtained stress ranges and number of cycles compared with the experimentally determined values.

Table 5.2 Predicted fatigue life and rebar stress range using proposed flowchart and equations

Specimen	N_{actual}	$\Delta\sigma_{needed}$ (MPa)	σ_{min} (MPa)	σ_{max} (MPa)	$\Delta\sigma_{provided}$ (MPa)	% of $\Delta\sigma_{needed}$	$N_{provided}$	% of $N_{actural}$
2	132794	145.14	108.17	249.84	141.67	97.6	192196	144.7
3 far	84800	156.30	108.17	249.84	141.67	90.6	136043	160.43
3 near	92100	133.56	108.17	249.84	141.67	106.1	110257	119.71
4	240500	78.10	98.07	226.51	128.44	164.5	145377	60.45
5	285000	73.45	98.07	226.51	128.44	174.9	153115	53.72
6	414700	60.72	95.40	220.34	124.95	205.8	146985	35.44
7	198400	83.16	95.40	220.34	124.95	150.2	139727	70.43

Below are the calculations, as described above, being solved for the values for Beam 4 in Table 5.2.

Fatigue Evaluation:

1) Critical crack length: $a_c = \frac{1}{\pi}\left(\frac{K_{IC}}{F*\sigma_{max}*}\right)^2 = \frac{1}{\pi}\left(\frac{113.35\ MPa\sqrt{m}}{2.368*250MPa}\right)^2 = 0.0117m$

Where K_{IC} was determined to be 133.35 MPa√m, F is calculated for the value of 0.0117m using Equation 2, and σ_{max}* is initially estimated at 250 MPa

2) The stress in the steel reinforcement which the FRP system needs to provide in order to achieve the desired fatigue life is calculated using the following equation. $\Delta\sigma_{needed} = \frac{\sqrt[m]{\frac{2\left(a_c\frac{2-m}{2} - a_i\frac{2-m}{2}\right)}{N(2-m)C}}}{F\sqrt{\pi}} = \frac{\sqrt[2.2375]{\frac{2\left(0.0117\frac{2-2.2375}{2} - 0.00218\frac{2-2.2375}{2}\right)}{240500(2-2.2375)1.43\times10^{-10}}}}{1.245\sqrt{\pi}} = 74.71MPa$

Where the determined values for C and m are used, N is the fatigue life from Figure 40 for Beam 4, the initial crack length measured in Beam 4 is used for a_i, and F is the average value between a_i and a_c. This value is slightly lower than the measured stress range for that specimen, which was 92.07 MPa. This suggests if the repair does produce a stress range in the steel reinforcement close to 74.71 MPa the fatigue life will be higher than what was found experimentally.

FRP Repair Design:

3) Section analysis of the Beam 4 solving for the ratio of depth of the neutral axis to reinforcement depth measured from the extreme compression fiber.

$0 = b*\frac{kd^2}{2} - n_sA_s(d-kd) - n_fA_f\left(d_f - kd\right) \rightarrow kd = 0.10138\ m$

Where the modular ratios, area of reinforcements, and depths to the reinforcements are the same as those used in Beam 4.

4) The service load stress in the steel reinforcement was calculated using Equation 10-14 from ACI 440.2 The stress at the lower load level (40kN) was: $\sigma_{min} = \frac{\left[M_D+\varepsilon_{bi}A_fE_f\left(d_f-\frac{kd}{3}\right)\right](d-kd)E_s}{A_sE_s\left(d-\frac{kd}{3}\right)(d-kd)+A_fE_f\left(d_f-\frac{kd}{3}\right)(d_f-kd)} =$

$$\frac{\left[28.8+0\times0.000194\times82047\left(0.34976-\frac{0.10183}{3}\right)\right](0.34925-0.10183)200000}{0.000852\times200000\left(0.34925-\frac{0.10183}{3}\right)(0.34925-0.10183)+0.000194\times82047\left(0.34976-\frac{0.10183}{3}\right)(0.34976-0.10183)}$$

$$= 98.067\ MPa$$

Where the strain in the concrete soffit is zero because the beams were not loaded prior to repair, and the dead load moment is from the lower level applied load and not just the self-weight of the beam.

5) The stress due to dead plus live load, 100kN, σ_{max} is calculated the same way, just with the dead plus live load moment. The calculated value is 226.509 MPa
6) The critical crack length from the *Fatigue Evaluation* side of the flowchart is then recalculated with the new max stress, which gave a value of 0.0142 m.
7) $\Delta\sigma_{needed}$ is revaluated with the new critical crack length and found to be 78.10 MPa, which is still below the experimentally measured value, but by a lesser amount.
8) The stress range provided by the FRP repair, $\Delta\sigma_{provided} = \sigma_{max} - \sigma_{min}$, was found to be 128.44 MPa. This is much higher than the needed value but also higher than the measured value.
9) $N_{provided} = \frac{2(a_c^{\frac{2-m}{2}} - a_i^{\frac{2-m}{2}})}{(2-m)C(F\Delta\sigma_{provided}\sqrt{\pi})^m} = \frac{2(0.0025^{\frac{2-2.2375}{2}} - 0.0024^{\frac{2-2.2375}{2}})}{(2-2.2375)1.43\times10^{-10}(0.72543\times128.44\sqrt{\pi})^{2.2375}} = 6055.5\ cycles$
The number of cycles to unstable crack growth using the $\Delta\sigma_{provided}$ was calculated for the growth of the fatigue crack from 0.0024m to 0.0025m. Applying the same process for 0.0001 m increments from the initial crack length to the critical crack length and summing the results together the total number of cycles to propagate the crack from can be found to be 145377.

These findings suggest the Paris Law can reasonably predict the fatigue life extension and *needed* stress range in the rebar for an FRP repaired RC girder; however, the presented equation from ACI 440.2 (Equation 13) shown in step 4) for determining the stress range in the rebar *provided* by an FRP repair produced values much higher (larger stress range) than what has been shown to take place. Therefore, further investigation into not only better determination of the Paris Law material constants, but also equations that can better predict the stresses in the steel reinforcement of RC girders with externally bonded FRP repairs is needed.

5.2 Future Work

The findings of the current study for fatigue life prediction and fatigue limit state design of FRP repaired RC flexural members emphasizes the need for continued research on this topic. Some of the most pressing needs requiring further study include:

- Evaluation of the recommended design flowchart against the results of other studies to determine any potential limitations of its applicability
- Determination of equations which can better estimate the steel reinforcement stress range in RC flexural members repaired with FRP
- Investigation into more accurate methods of measuring the fatigue crack length and growth rate to achieve a more accurate determination of the Paris Law constants for steel reinforcing bars
- The presence of environmental conditions (corrosion, embedded in concrete) of the reinforcing steel potentially altering the fracture toughness and Paris Law constants
- Determining statistical variations in the Paris Law constants for different rebar types, repair systems, and environmental conditions to determine if a single value can be used for each coefficient
- Adjusting the recommended flowchart to include prestressed externally bonded CFRP

5.3 Summary

The current study used a unique experimental test to directly measure the fatigue crack propagation rates in the tensile steel reinforcement of full scale RC beams with and without CFRP repairs. The results of the tests were then used to determine the material constants in the Paris Law equation. Use of the Paris Law equation along with equations from ACI 440.2 allowed for the development of a design process with which an engineer can design an FRP repair, extending the fatigue life of the strengthened RC flexural member by ensuring the fatigue crack will never reach its critical value within the design life. This design philosophy is unlike those of current design provisions, which recommend an overly conservative design that prohibits any fatigue crack growth. Additional significant findings/unique characteristics of the study include:

- The application of both CFRP systems lowered the stress range in the tensile reinforcement. Specifically, Beams 6 and 7, which were strengthened with the Tyfo UC strips, achieved the lowest stress range with Beams 4 and 5 strengthened with the Tyfo SCH-41 sheets producing just a slightly higher stress range. The lowered stress ranges in all repaired beams produced extended fatigue lives in these beams over the unrepaired specimens.
- A visual method of inspection for fatigue crack growth in the tensile steel reinforcing bars of RC beams, despite affecting the structural performance of the beam to a minor degree, generated accurate crack growth rate results producing Paris Law material constant values fairly close to well-accepted values. Variation in theses coefficient values from published values may have occurred due to the visual method not being able to give the absolute crack length value as the forefront of the crack was at the center of the bar and the measured crack length was slightly shorter due to the curvature of the crack front.
- The use of the Paris Law equation with well-established constant values, on average, vastly underestimated (12.6% of actual) the stable crack growth fatigue life of an RC flexural member strengthened with FRP in this study; however, the use of experimentally determined material constant values (m=2.24 and C = 1.435E^{-10}), on average, increased the accuracy but produced an overestimation (163% of actual) of the fatigue life.
- Calculations using section analysis and equations from ACI 440.2 showed a difference in the fatigue life in beams that are strengthened to the same level yet using different CFRP strengthening systems, suggesting a difference between repairing a RC flexural member for strength and for fatigue. However, experimental results were inconclusive in support of this hypothesis, with one of the Tyfo UC strip strengthened beams, which should have had a longer fatigue life, in fact fatiguing faster than the two Tyfo SCH-41 sheet strengthened beams.
- A design flowchart based on a fatigue limit state was established using the Paris Law and already developed equations for strength design of FRP repairs. On average, the predicted stable crack growth fatigue life using this flowchart was 92% of the actual fatigue life determined from the experimental study, suggesting it reasonably captures the fatigue crack growth and can potentially be used in the future.

BIBLIOGRAPHY

AASHTO. AASHTO LFRD bridge design specifications (SI units), 6th ed. (2012). Washington DC, USA: American Association of State Highway and Transportation Officials.

ACI Committee 215. *Considerations for design of concrete structures subjected to fatigue loading.* ACI-215R-74 (reapproved 1997). Farmington Hills, Mich., USA: American Concrete Institute, 1974.

ACI Committee 440. *Guide for the Design and Construction of Externally Bonded FRP Systems for Strengthening Concrete Structures.* ACI 440.2R-08. Farmington Hills, Mich., USA: American Concrete Institute, 2008.

Aidoo, J., Harries, K. A., and Petrou, M. F. (2004). "Fatigue behavior of carbon fiber reinforced polymer strengthened reinforced concrete bridge girders." *Journal of Composites for Construction*, 8(6), 501-509.

Aidoo, J., Harries, K. A., and Petrou, M. F. (2006). "Full-scale experimental investigation of repair of reinforced concrete interstate bridge using CFRP materials." *Journal of Bridge Engineering*, 11(3), 350-358.

Al-Rousan, R., and Issa, M. (2011). "Fatigue performance of reinforced concrete beams strengthened with CFRP sheets." *Construction and Building Materials*, 25, 3520-3529.

American Society for Testing and Materials. *Standard Test Methods for Notched Bar Impact Testing of Metallic Materials. ASTM E-23-12c.* E28 Committee, 2007.

ASCE. 2013 *Report Card for America's Infrastructure,* American Society of Civil Engineers, 2013.

Badawi, M. A. (2007). "Monotonic and fatigue flexural behavior of RC beams strengthened with prestressed NSM CFRP rods." Ph.D. thesis, University of Waterloo, Waterloo, Ontario, Canada, 2007.

Bank, L.C. (2006). *Composites for Construction: Structural Design with FRP Materials.* John Wiley & Sons, Inc.

Barnes, R. A., and Mays, G. C. (1999). "Fatigue performance of concrete beams strengthened with CFRP plates." *Journal of Composites for Construction*, 3(2), 63-72.

Barsom, J. M., and Rolfe, S. T. *Fracture and Fatigue Control in Structures – Applications of Fracture Mechanics.* Butterworth-Heinemann, Woburn, MA. 1999.

British Standards Institution. *Guide to methods for assessing the acceptability of flaws in metallic structures*. BS 7910, 2013.

Dong, Y., Ansari, F., and Karbhari, V.M. (2008). "Fatigue performance of reinforced concrete beams with externally bonded CFRP reinforcement." *Structure and Infrastructure Engineering*.

Derkowski, W. (2006). "Fatigue life of reinforced concrete beams under bending strengthened with composite materials." *Archives of Civil and Mechanical Engineering*, 6(4), 33-47.

Dowling, N. (1999). *Mechanical behavior of materials: Engineering methods for deformation, fracture and fatigue*. (2nd ed.). Upper Saddle River, NJ: Prentice-Hall, Inc.

Ekenel, M., Rizzo, A., Myers, J. J., and Nanni, A. (2006). "Flexural fatigue behavior of reinforced concrete beams strengthened with FRP fabric and precured laminate systems." *Journal of Composites for Construction,* 10(5), 433-442.

El-Hacha, R., Wight, R. G., Heffernan, P. J., and Erki, M. A. (2003). "Prestressed CFRP sheets for strengthening reinforced concrete structures in fatigue." Proceedings from 6th International Symposium on Fiber-Reinforced Polymer (FRP) Reinforcement for Concrete Structures (FRPRCS-6), Vol. 1, Singapore, 895-904.

Fisher, J. W., Albrecht, P. A., Yen, B. T., Kingerman, D .J., and McNamee, B. M. (1974). "Fatigue strength of steel beams with welded stiffeners and attachments." *NCHRP Rep. 147*, National Cooperative Highway Research Program, Transportation Research Board, Washington, DC.

Frost, N.E., Marsh, K.J., and Pook, L.P. (1974) *Metal Fatigue.* Clarendon Press.

Gordon, K., and Cheng, L. (2011). "Evaluation of empirical fatigue prediction models for FRP-strengthened RC beams." *ACI Special Publications S275-37*, 275, 1-14.

Gussenhoven, R., and Brena, S. F. (2005). "Fatigue behavior of reinforced concrete beams strengthened with different FRP laminate configurations." *Fiber-reinforced polymer (FRP) reinforcement for concrete structures (SP-230),* ACI, 613-630.

Heffernan, P. J., and Erki, M. A. (2004). "Fatigue behavior of reinforced concrete beams strengthened with carbon fiber reinforced plastic laminates." *Journal of Composites for Construction,* 8(2), 132-140.

Jumaat, M. Z., and Alam, M. A. (2007). "Plate bonded strengthened RC beams with end and intermediate anchors." *International Journal of Engineering and Technology*, 4(2), 185-193.

Kim, Y. J., and Heffernan, P. J. (2008). "Fatigue behavior of externally strengthened concrete beams with fiber-reinforced polymers: State of the art." *Journal of Composites for Construction,* 12(3), 246-256.

Lovegrove, J.M., Salah El Din, A.S., and Daoud, O.K. (1979). "Fatigue Crack Growth in the Tension Steel of Reinforced Concrete." *Fatigue of Engineering Materials and Structures*, 1, 173-183.

Masoud, S., Soudki, K., and Topper, T. (2001). "DFRP-strengthened and corroded RC beams under monotonic and fatigue loads." *Journal of Composite Construction,* 5(4). 228-236.

Milan, M. T., Spinelli, D., Bose Filho, W. W., Montezuma, M. F. and V., Tita, V. (2004). "Failure analysis of a SAE 4340 steel locking bolt." *Engineering Failure Analysis*, 11, 915-924.

Nordtest Method. (1988). "Crack depth measurement: Electrical potential drop techniques." (NT NDT 006) Norden.

Oudah, F. and El-Hacha, R. (2012). "Research progress on the fatigue performance of RC beams strengthened in flexure using fiber reinforced polymers." *Composites: Part B*, 47, 82-95.

Papakonstantinou, C. G., Petrou, M. F., and Harries, K. A. (2001). "Fatigue behavior of RC beams strengthened with GFRP sheets." *Journal of Composites for Construction,* 5(4), 246-253.

Paris, P. C., (1964). "The fracture mechanics approach to fatigue." 10th Sagamore Army Material Research Conference, Syracuse University Press.

Rocha, M., Brühwiler, E. (2012). “Prediction of fatigue life of reinforced concrete bridges using fracture mechanics.” *Bridge Maintenance, Safety, Management, Resilience and Sustainability*, 3755-3760.

Shah, S. G., and Chandra Kishen, J. M. (2012). “Use of acoustic emissions in flexural fatigue crack growth studies on concrete.” *Engineering Fracture Mechanics*, 87, 36-47.

Shahawy, M., and Beitelman, T. E. (1999). “Static and fatigue performance of RC beams strengthened with CFRP laminates.” *Journal of Structural Engineering*, 125(6), 613-621.

Toutanji, H., Zhao, L., Deng, Y., Zhang, Y., and Balaguru, P. (2006). “Cyclic behavior of RC beams strengthened with carbon fiber sheets bonded by inorganic matrix.” *Journal of Materials in Civil Engineering*, 18(1), 28-35.

Zheng, H., and Abel, A. (1998). “Stress concentration and fatigue of profiled reinforcing steels.” *International Journal of Fatigue*, 20(10), 767-773.

APPENDIX A. MATERIAL PROPERTIES

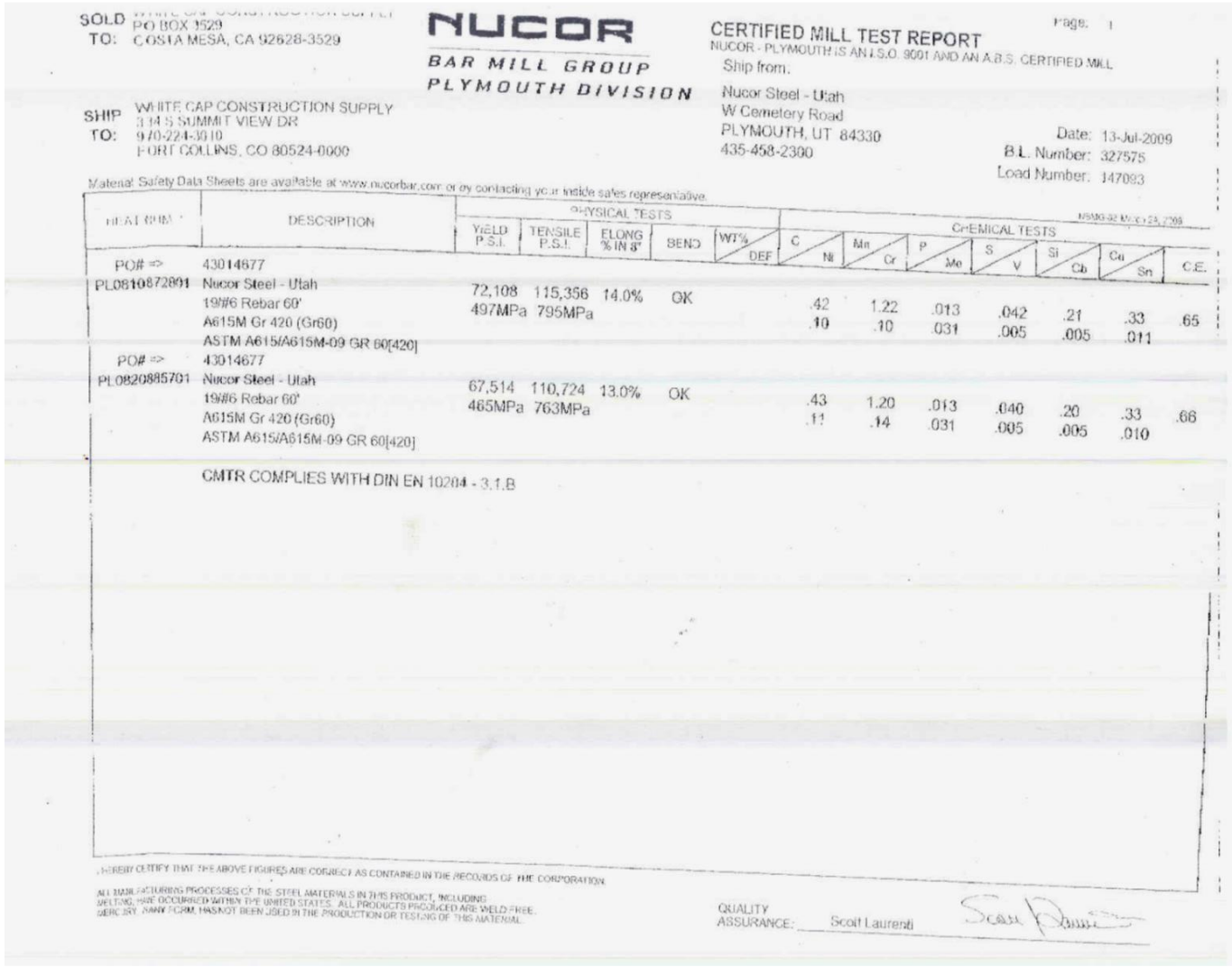

SOLD TO: PO BOX 3529
COSTA MESA, CA 92628-3529

SHIP TO: WHITE CAP CONSTRUCTION SUPPLY
3345 SUMMIT VIEW DR
970-224-3010
FORT COLLINS, CO 80524-0000

NUCOR
BAR MILL GROUP
PLYMOUTH DIVISION

CERTIFIED MILL TEST REPORT

Page: 1

NUCOR - PLYMOUTH IS AN I.S.O. 9001 AND AN A.B.S. CERTIFIED MILL

Ship from:
Nucor Steel - Utah
W Cemetery Road
PLYMOUTH, UT 84330
435-458-2300

Date: 13-Jul-2009
B/L Number: 327575
Load Number: 147093

Material Safety Data Sheets are available at www.nucorbar.com or by contacting your inside sales representative.

NSMD-32 Mod 23, 2009

HEAT (HEAT)	DESCRIPTION	PHYSICAL TESTS YIELD P.S.I.	TENSILE P.S.I.	ELONG % IN 8"	BEND	WT% DEF	CHEMICAL TESTS C / Ni	Mn / Cr	P / Mo	S / V	Si / Cb	Cu / Sn	C.E.
PO# =>	43014677												
PL0810872891	Nucor Steel - Utah 19/#6 Rebar 60' A615M Gr 420 (Gr60) ASTM A615/A615M-09 GR 60[420]	72,108 497MPa	115,356 795MPa	14.0%	OK		.42 .10	1.22 .10	.013 .031	.042 .005	.21 .005	.33 .011	.65
PO# =>	43014677												
PL0820885701	Nucor Steel - Utah 19/#6 Rebar 60' A615M Gr 420 (Gr60) ASTM A615/A615M-09 GR 60[420]	67,514 465MPa	110,724 763MPa	13.0%	OK		.43 .11	1.20 .14	.013 .031	.040 .005	.20 .005	.33 .010	.66

CMTR COMPLIES WITH DIN EN 10204 - 3.1.B

I HEREBY CERTIFY THAT THE ABOVE FIGURES ARE CORRECT AS CONTAINED IN THE RECORDS OF THE CORPORATION.

ALL MANUFACTURING PROCESSES OF THIS STEEL MATERIALS IN THIS PRODUCT, INCLUDING MELTING, HAVE OCCURRED WITHIN THE UNITED STATES. ALL PRODUCTS PRODUCED ARE WELD FREE. MERCURY, IN ANY FORM, HAS NOT BEEN USED IN THE PRODUCTION OR TESTING OF THIS MATERIAL.

QUALITY ASSURANCE: Scott Laurenti

SOLD TO: WHITE CAP CONSTRUCTION SUPPLY
PO BOX 3529
COSTA MESA, CA 92628-3529

SHIP TO: WHITE CAP CONSTRUCTION SUPPLY
334 S. SUMMIT VIEW DRIVE
970-224-3010
FORT COLLINS, CO 80524-

NUCOR
NUCOR CORPORATION
NUCOR STEEL UTAH

CERTIFIED MILL TEST REPORT

NUCOR - PLYMOUTH IS AN I.S.O. 9001 AND AN A.B.S. CERTIFIED MILL

Ship from:
Nucor Steel - Utah
W Cemetery Road
PLYMOUTH, UT 84330
435-458-2300

Date: 15-Jul-2011
B.L. Number: 380328
Load Number: 198138

Material Safety Data Sheets are available at www.nucorbar.com or by contacting your inside sales representative.

NBMG-08 March 9, 2011

HEAT NUM *	DESCRIPTION	PHYSICAL TESTS					CHEMICAL TESTS							
		YIELD P.S.I.	TENSILE P.S.I.	ELONG % IN 8"	BEND	WT% DEF	C / Ni	Mn / Cr	P / Mo	S / V	Si / Cb	Cu / Sn	C.E.
PO# =>	43045421												
PL1110404801	Nucor Steel - Utah	69,612	103,464	15.0%	OK	.8%	.39	.93	.016	.036	.25	.26	.57
	10/#3 Rebar 20' 2K	480MPa	713MPa				.09	.15	.021	.005	.005		
	A615M GR 420 (Gr60)												
	ASTM A615/A615M-09b GR 60[420]												
	AASHTO M31-07												
PO# =>	43045421												
PL1120416001	Nucor Steel - Utah	72,820	107,823	16.0%	OK	1.9%	.39	.97	.013	.036	.27	.31	.58
	10/#3 Rebar 20' 2K	502MPa	743MPa				.11	.15	.027	.005	.005		
	A615M GR 420 (Gr60)												
	ASTM A615/A615M-09b GR 60[420]												
	AASHTO M31-07												

CMTR COMPLIES WITH DIN EN 10204 - 3.1.B

I hereby certify that the material described herein has been manufactured in accordance with the specifications and standards listed above and that it satisfies those requirements.
1.) Weld repair was not performed on this material.
2.) Melted and Manufactured in the United States.
3.) Mercury, Radium, or Alpha source materials in any form have not been used in the production of this material.

QUALITY ASSURANCE Scott Laurenti